Divergence in Climate Model Projections of Future Arctic Atlantification

MORVEN MUILWIJK,[a,b] ALEKSI NUMMELIN,[c] CÉLINE HEUZÉ,[d] IGOR V. POLYAKOV,[e] HANNAH ZANOWSKI,[f] AND LARS H. SMEDSRUD[b]

[a] *Norwegian Polar Institute, Tromsø, Norway*
[b] *Geophysical Institute, University of Bergen and Bjerknes Centre for Climate Research, Bergen, Norway*
[c] *Norwegian Research Centre and Bjerknes Centre for Climate Research, Bergen, Norway*
[d] *Department of Earth Sciences, University of Gothenburg, Gothenburg, Sweden*
[e] *International Arctic Research Center and College of Natural Sciences and Mathematics, University of Alaska Fairbanks, Fairbanks, Alaska*
[f] *Department of Atmospheric and Oceanic Sciences, University of Wisconsin–Madison, Madison, Wisconsin*

(Manuscript received 12 May 2022, in final form 3 November 2022)

ABSTRACT: The Arctic Ocean is strongly stratified by salinity in the uppermost layers. This stratification is a key attribute of the region as it acts as an effective barrier for the vertical exchanges of Atlantic Water heat, nutrients, and CO_2 between intermediate depths and the surface of the Eurasian and Amerasian basins (EB and AB, respectively). Observations show that from 1970 to 2017, the stratification in the AB has strengthened, whereas, in parts of the EB, the stratification has weakened. The strengthening in the AB is linked to freshening and deepening of the halocline. In the EB, the weakened stratification is associated with salinification and shoaling of the halocline (Atlantification). Simulations from a suite of CMIP6 models project that, under a strong greenhouse gas forcing scenario (ssp585), the overall surface freshening and warming continue in both basins, but there is a divergence in hydrographic trends in certain regions. Within the AB, there is agreement among the models that the upper layers will become more stratified. However, within the EB, models diverge regarding future stratification. This is due to different balances between trends at the surface and trends at depth, related to Fram Strait fluxes. The divergence affects projections of the future state of Arctic sea ice, as models with the strongest Atlantification project the strongest decline in sea ice volume in the EB. From these simulations, one could conclude that Atlantification will not spread eastward into the AB; however, models must be improved to simulate changes in a more intricately stratified EB correctly.

KEYWORDS: Arctic; Freshwater; Surface layer; Ocean models; Coupled models; Mixing

1. Introduction

Much of the present-day central Arctic Ocean is a so-called beta ocean—it is strongly stratified by salinity, unlike subtropical seas where the upper layers are stratified by temperature (Nansen 1902; Carmack 2007). Over the last few decades, the Arctic region has experienced surface warming at more than twice the global rate (Cohen et al. 2020; IPCC 2021), and an intensive loss of Arctic sea ice and glacial ice (Stroeve and Notz 2018; Shepherd et al. 2020). These changes are associated with increased freshwater fluxes into the upper ocean (Solomon et al. 2021, and references therein), and changes in the intermediate and deeper layers (Årthun and Eldevik 2016). Even if the increasing trend in freshwater input to the Arctic Ocean is projected to continue (Zanowski et al. 2021), a stronger subpolar influence (borealization; Polyakov et al. 2020a) and the simultaneous loss of sea ice (Notz and SIMIP Community 2020) make the expected stratification changes nontrivial. Here, we aim to provide an overview of the changing Arctic stratification using unique historical observations and a range of future model projections.

Typically, the upper part of the water column in the deep Arctic basins [the Eurasian Basin (EB) and Amerasian Basin (AB)] is characterized by two distinct layers: A fresh and cold surface layer and a warmer and saline layer at depth with water of Atlantic origin (Rudels 2015). There is a cold halocline between them where the salinity increases rapidly with depth. This stratification is one of the essential attributes of the Arctic Ocean, acting as an effective barrier for water mass mixing and hence vertical exchanges (Peralta-Ferriz and Woodgate 2015). The strong layering effectively shields the sea ice cover from oceanic heat found at depth (Nansen 1902; Aagaard et al. 1981), limits primary production due to reduced nutrient fluxes (Randelhoff et al. 2020), and reduces the

Denotes content that is immediately available upon publication as open access.

Supplemental information related to this paper is available at the Journals Online website: https://doi.org/10.1175/JCLI-D-22-0349.s1.

Nummelin's additional affiliation: Finnish Meteorological Institute, Helsinki, Finland.

Corresponding author: Morven Muilwijk, morven.muilwijk@npolar.no

DOI: 10.1175/JCLI-D-22-0349.1

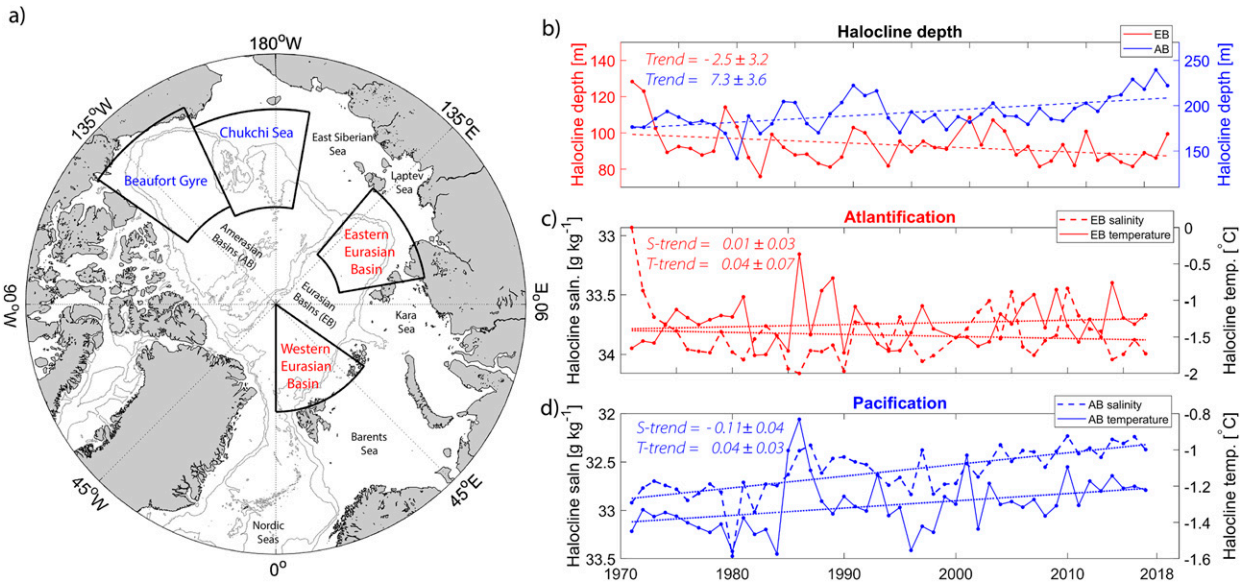

FIG. 1. (a) Arctic Ocean map with identified regions. Western Eurasian basin region, Eastern Eurasian basin region, Chukchi Sea region, and Beaufort Gyre region are indicated. Light gray contour lines show the 500- and 2000-m isobaths from ETOPO1 bathymetry (Amante and Eakins 2009). (b) Observed annual mean depth of halocline base in the Eurasian basin (EB; red) and Amerasian basin (AB; blue) regions. Observed annual mean temperature (solid line) and salinity (dashed line) averaged over the halocline layer in the (c) EB region and (d) AB region. Trend values are given per decade.

ocean's capability to take up atmospheric CO_2 (Yasunaka et al. 2018). The warm and saline Atlantic Water (AW) at intermediate depth enters the central Arctic Ocean via the deep Fram Strait and the shallow Barents Sea and circulates cyclonically in the Arctic interior, controlled by topography (Timmermans and Marshall 2020; Bluhm et al. 2020). The Atlantic inflow is the primary heat source for the Arctic Ocean, although Pacific Water (PW) is an important source of oceanic heat and relatively freshwater in the Pacific sector, especially in summer (Woodgate et al. 2012). The PW contributes to the low salinity in the uppermost layer (~250 m) of the AB (Proshutinsky et al. 2009, 2019). In contrast, in other Arctic regions, the major contributions of freshwater input to the surface mixed layer (SML) stem from precipitation (Serreze et al. 2006), freshwater runoff from rivers (Holmes et al. 2012), glacial ice melting (Haine et al. 2015), and melting of sea ice (Haine et al. 2015; Wang et al. 2019). The Arctic Ocean's major outflows carrying cold and fresh Polar Water (Timmermans and Marshall 2020) occur through the Canadian Archipelago and the western part of Fram Strait.

The volume transport and temperature of AW entering the EB have increased (Tsubouchi et al. 2021; Smedsrud et al. 2022) and now play a greater role in sea ice loss in the Eurasian sector of the Arctic (Carmack et al. 2015). Although the AW inflow historically has been significant for regulating the sea ice cover in the Barents Sea and Western EB (Årthun et al. 2012; Onarheim et al. 2015), its impact on sea ice has recently expanded toward the Eastern EB, a process often referred to as "Atlantification" (Polyakov et al. 2017). Simultaneously, an anomalous advection of warm and relatively fresh PW has been observed, resulting in a recent change called "Pacification" (Polyakov et al. 2020a). The combined effect of both processes is referred to as a "borealization" (Polyakov et al. 2020a), a shift in the northward range and associated ecosystem of the Arctic Ocean, which includes changes in both the physical, geochemical, and biological components. The hydrographic changes related to Atlantification and Pacification are expressed regionally and have opposite effects on stratification [see Fig. 1 herein and Polyakov et al. (2020a)]. Pacification is mainly associated with the AB and an anomalous influx of PW. Generally, anomalous advection of PW sharpens the density gradient and results in a strengthened stratification in the AB (Steele et al. 2004). Atlantification has been manifested by a local surface layer salinification and, therefore, a weakening of the halocline and warming and shoaling of the AW layer below (Fig. 1 herein and Polyakov et al. 2020b). This results in an overall weakened stratification in the EB. These conditions are more susceptible to increased vertical mixing and thus favor biological production by bringing up nutrients (Polyakov et al. 2020a). Another essential local process is the general freshening of the upper EB and AB (Haine et al. 2015; Haine 2020; Solomon et al. 2021), which has resulted in a strengthened stratification (Li et al. 2020), especially in the AB (Polyakov et al. 2020a). The AB holds the largest reservoir of liquid freshwater in the Arctic, as the circulation in the Beaufort Gyre, sustained by the anticyclonic winds, drives Ekman convergence and deepens the halocline within the gyre (Proshutinsky et al. 2002). Since the mid-1990s, hydrographic and satellite observations have shown increases and redistribution of freshwater in the Arctic (Rabe et al. 2011; Proshutinsky et al. 2019, and references therein). The increases have been linked to a combination of an intensification of the large-scale atmospheric forcing over the Beaufort Gyre (Giles et al. 2012; Proshutinsky et al.

2019; Cornish et al. 2020), increased river runoff (Peterson et al. 2002; Rabe et al. 2014; Haine et al. 2015), increased flux of freshwater through Bering Strait (Woodgate et al. 2005) and direct contributions of sea ice melt (Wang et al. 2019). A recent review by Solomon et al. (2021) has, however, shown that the trend in total Arctic freshwater content in the 2010s has stabilized somewhat relative to the 2000s due to an increased compensation between a freshening of the Beaufort Gyre and a reduction in freshwater in the rest of the Arctic Ocean. Nonetheless, as the Arctic is expected to continue warming in response to emissions (Davy and Outten 2020), the freshwater fluxes into to the Arctic Ocean are projected to increase (e.g., Holland et al. 2007; Kattsov et al. 2007; Jahn and Laiho 2020; Zanowski et al. 2021; Wang et al. 2022), partly reflecting an intensification of the hydrological cycle (Held and Soden 2006; Haine 2020), and partly due to increased river runoff (Haine 2020). The freshwater flux due to melting sea ice has been a large contributor to the recent freshening, but is likely to decrease into the future, and become relatively small by the second half of the twenty-first century, as less ice is available to melt (Shu et al. 2018). Experiments with column models (Nummelin et al. 2015; Davis et al. 2016) and a global climate model (Nummelin et al. 2016) have examined the potential effects of increased river runoff, and they find that the Arctic stratification will increase and that the freshwater has a larger effect than elevated wind-driven mixing (Davis et al. 2016). However, these studies do not consider other freshwater sources, the regional aspect, or the opposing effects of Atlantification. For example, using a single climate model (HiGEM), Lique et al. (2018) showed that under an extreme global warming scenario, the stratification in this model is strongly enhanced in the AB but reduced in the EB.

It is well known that climate models experience crucial biases in simulated Arctic hydrography. This is true for both ocean–sea ice only models (Ilicak et al. 2016; Wang et al. 2016; Tsujino et al. 2020) and fully coupled climate models, such as the ones participating in the Climate Model Intercomparison Project phase 5 (CMIP5; Shu et al. 2019) and phase 6 (CMIP6; Khosravi et al. 2022; Rosenblum et al. 2021). More specifically, the models struggle to represent AW circulation and mixing processes in the central Arctic Ocean (Ilicak et al. 2016; Tsujino et al. 2020), have significant differences in circulation as a response to similar forcing (Muilwijk et al. 2019), and have a large spread in projections of sea ice cover (Shu et al. 2020). Despite these shortcomings, climate models are useful tools to investigate the competing processes mentioned above and evaluate how they will change into the future.

Khosravi et al. (2022) recently published an overview of biases in the Atlantic Water layer in the models that participated CMIP6. Their results indicate that biases persist from CMIP5 to CMIP6. Our companion paper, Heuzé et al. (2023), expanded on their results by also assessing the deep and bottom waters and by explaining the causes for all these biases, focusing primarily on the models' mean historical state. Additionally, Arctic freshwater storage and fluxes in a subset of the CMIP6 models have been analyzed by Zanowski et al. (2021) and Wang et al. (2022), and the sea ice in CMIP6 models has been assessed by Notz and SIMIP Community (2020) and Shen et al. (2021). Rosenblum et al. (2021) carefully examined two versions of one model (CESM1 and CESM2) in one region of the Arctic, but until now, no study has investigated hydrographic trends and stratification in multiple models and regions. We address this gap with a pan-Arctic examination of 14 CMIP6 models against the observations. Using a unique 48-yr archive of observations (1970–2017), we first synthesize the observed changes in different regions of the Arctic Ocean before comparing them to the historical simulations. We then describe how the stratification and hydrography in these regions are projected to change under a high (ssp585) emission scenario (O'Neill et al. 2016) and how this is related to changes in sea ice cover.

This manuscript is structured as follows: We start by describing the observational and model data used in this study and present a new diagnostic used to evaluate integral changes in Arctic Ocean stratification (section 2). We then compare observed and simulated stratification in recent decades (section 3a) before we investigate the future trends (sections 3b and 3c) and finally discuss the mechanisms responsible for these changes (section 3d) and the impacts on sea ice (section 3e). We focus particularly on the role of advective contra local processes and finish with a summary of our findings and a discussion on the broader implications of our work (section 4).

2. Data and methods

a. *Observational data*

This study uses a unique historical archive of hydrographic observations from 1970 to 2017, including Russian, American, Canadian, and European ship and aircraft expeditions, year-round crewed drift stations, autonomous drifters, and submarine data. This is an updated version of the archive previously used by, for example, Polyakov et al. (2020a) to investigate long-term AW variability and halocline stability, and has been made available through the Arctic Data Center (Muilwijk and Polyakov 2022). The temporal and spatial coverage for the data used in this study is shown in Fig. S1 in the online supplemental material. Unfortunately, historical observations of the Arctic Ocean are generally sparse and have limited spatial coverage. Especially in the 1990s, data coverage is not good, and in general, there have been few winter campaigns in the central basins. However, autonomous Ice-Tethered Profilers (ITP), crewed ice-drift stations, and some ship-based campaigns ensure a relatively good seasonal coverage in later decades (Fig. S2). The bulk of historical data was gathered to construct the climatological atlases of the Arctic Ocean by Gorshkov (1980), Treshnikov (1985), and Timokhov and Tanis (1997). Before 1980 most observations used Nansen bottles to measure salinity, while modern and more accurate conductivity–temperature–depth (CTD) instruments became more common as the use of icebreakers and submarines increased in the 1980s and 1990s. The typical accuracy of measurements from the Nansen bottles was estimated by Timokhov and Tanis (1997) to be 0.01°C for temperature and 0.02 for salinity. Since the 2000s, a major part of the data stems from ship-based measurements complemented by drifting ITPs, which autonomously collect

TABLE 1. Characteristics of the 14 CMIP6 models used in this study: horizontal grid type, horizontal resolution in the Arctic, type of vertical grid and number of vertical levels, ocean model component, parameter used to calculate sea ice volume, and reference. Note that the vertical layers do not have uniform thickness and that the vertical resolution is higher near the surface and lower at depth. The horizontal resolution in the Arctic (third column) was calculated as the square root of the total area north of 70°N divided by the number of points the model has north of 70°N. For the vertical grids, ρ means isopycnic; σ terrain-following; and multiple symbols mean hybrid.

Model	Grid type	Resolution (km)	Vertical grid (No. of levels)	Ocean model	Ice parameter	Reference
BCC-CSM2-MR	Tripolar	54	z (40)	MOM4-L40v2	sivol	Wu et al. (2019)
CAMS-CSM1-0	Tripolar	54	z (50)	MOM41	sivol	Xin-Yao et al. (2019)
CanESM5	Tripolar	50	z (45)	NEMO3.4.1	simass	Swart et al. (2019)
CESM2	Rotated	41	z (60)	POP2	sithick	Danabasoglu et al. (2020)
EC-Earth3	Tripolar	49	z^* (75)	NEMO3.6	sithick	Döscher et al. (2021)
GFDL-CM4	Tripolar	9	ρ–z^* (75)	MOM6	sivol	Adcroft et al. (2019)
GFDL-ESM4	Tripolar	18	ρ–z^* (75)	MOM6	sivol	Dunne et al. (2020)
GISS-E2-1-H	Regular	46	ρ–z–σ (32)	Hycom	sivol	Kelley et al. (2020)
IPSL-CM6A-LR	Tripolar	49	z^* (75)	NEMO3.2	sivol	Lurton et al. (2020)
MIROC6	Tripolar	39	z–σ (62)	COCO4.9	sivol	Tatebe et al. (2019)
MPI-ESM1-2-HR	Tripolar	36	z (40)	MPIOM1.63	sivol	Müller et al. (2018)
MRI-ESM2-0	Tripolar	39	z^* (60)	MRI.COMv4	sivol	Yukimoto et al. (2019)
NorESM2-LM	Tripolar	38	ρ–z (53)	BLOM (MICOM)	sivol	Seland et al. (2020)
UKESM1-0-LL	Tripolar	50	z^* (75)	NEMO3.6	sivol	Sellar et al. (2020)

CTD profiles down to 800 m. For consistency and direct comparison with model data we present salinity and temperature in practical salinity units (psu) and potential temperature. All analysis is based on annual mean profiles. We use the TEOS10 equation of state as implemented in the Gibbs-SeaWater (GSW) Oceanographic Toolbox (McDougall and Barker 2011) to calculate density.

b. The CMIP6 models

We use the output from 14 fully coupled models that participated in the Climate Model Intercomparison Project phase 6 (CMIP6; Eyring et al. 2016), listed in Table 1. For comparison, these models are the same as those used in our companion paper (Heuzé et al. 2023) and were selected from the 35 CMIP6 models used in Heuzé (2021) as representative of their family, for diversity in vertical grid types and after eliminating the ones with the poorest bathymetry. Typical horizontal model resolution is ~50 km in the Arctic (9 km for the highest resolution) and 50 levels or more in the vertical. No more than two models share the same ocean component with the same version (Table 1).

We evaluated the last 45 years of the historical run (i.e., January 1970–December 2014) and the first 85 years of the future high (ssp585) emission scenario (Eyring et al. 2016) (i.e., January 2015–December 2100). The strong forcing scenario was chosen to clearly isolate climate change signals from internal variability. Trends were calculated from 1970 to 2014 to match the observational data and over 2015–70 for the future scenario. Trends are not calculated over the full future period because the changes we observe are transient, and there is some flattening toward the end of the century (section 3b). For the sea ice analysis presented in section 3e, the trends are calculated over the 2015–45 period. For each model, only one ensemble member was used: "r1i1p1f1" for the majority of models and "r1i1p1f2" when r1i1p1f1 was not available (GISS-E2-1-H and UKESM1-0-LL). The simulated internal variability is not investigated in detail, and we note that under the high forcing scenario this is less important, whereas for the 1970–2014 period, forcing is modest and internal variability could play an important role. All trends presented are statistically significant unless otherwise stated. The output we used are the monthly seawater practical salinity "so", potential temperature "thetao", and sea ice concentration "siconc" and thickness "sivol/sithick" or sea ice mass "simass" (Table 1). Water density was calculated using the TEOS10 equation of state as implemented in the GSW Oceanographic Toolbox (McDougall and Barker 2011). All computations were performed on the models' native grid before being averaged for each of the four regions shown in Fig. 1.

c. Methods

The primary objective of this paper is to quantify trends in stratification. Traditionally, stratification has been quantified using the Brunt–Väisälä buoyancy frequency $N^2 = -(g/\rho_0)\delta\rho/\delta z$, where ρ is potential density, ρ_0 is a reference density, and g is the gravitational acceleration. This parameter provides a profile of stability between points in the vertical but does not yield a bulk measure of the stability within a layer (Polyakov et al. 2018). The upper part of the EB and AB water column features complex layering. It consists of a surface mixed layer (SML; ~20–50 m) overlaying the halocline, characterized by cold temperatures and a very high salinity gradient (~50–250 m), and a warmer (temperature $>$ 0°C) and more saline layer of AW below (Rudels et al. 2004). Traditionally, the definition of AW is based on temperature, salinity, or density values. However, since we expect these properties to be biased in the models, we instead chose to define the AW core as the depth of the temperature maximum below 100 m. When we

further refer to AW properties, we thus refer to the properties at the depth of the AW core. According to Heuzé et al. (2023), the CMIP6 multimodel mean AW core depth is approximately 400 m in the EB and approximately 530 m in the AB but varies substantially from model to model (ranging between 77 and 1300 m).

The halocline is often divided into a cold halocline, with near-freezing temperatures, and lower halocline waters, with increasing temperature and salinity with depth (Steele et al. 1989; Rudels et al. 2004). Polyakov et al. (2018) noted that, especially within the halocline, which consists of a complex combination of water masses with varying effects on stratification (Bluhm et al. 2015), N^2 is insufficient as a measure of stratification since it does not provide a bulk metric. Also, a simple density contrast between two levels ($\Delta\sigma_\theta$) is similarly insufficient. Polyakov et al. (2018) therefore proposed available potential energy (APE) as a good integral indicator of changes in stratification in the combined SML and halocline layer. For each profile, APE is calculated as

$$\mathrm{APE} = \int_{H_{\mathrm{halo}}}^{\mathrm{surface}} g(\rho - \rho_{\mathrm{halo}}) z \, dz, \tag{1}$$

where H_{halo} is the depth of the lower boundary of the halocline and ρ_{halo} is the potential density at that lower boundary of the halocline.

In observations, the lower boundary of the halocline is usually determined using a density ratio algorithm following the method proposed by Bourgain and Gascard (2011), which was also used by, for example, Polyakov et al. (2018) and Metzner et al. (2020). Following Bourgain and Gascard (2011), such density ratio is defined as

$$R_\rho = \left| \left(\alpha \frac{\delta \Theta}{\delta z} \right) \Big/ \left(\beta \frac{\delta S_{\mathrm{A}}}{\delta z} \right) \right|, \tag{2}$$

where α is the thermal expansion coefficient, β is the haline contraction coefficient, Θ is the Conservative Temperature, and S_{A} is the Absolute Salinity. The lower boundary of the halocline H_{halo} is then defined as the depth where R_ρ exceeds the threshold of 0.05, which was determined empirically from observations in the Arctic (Bourgain and Gascard 2011).

Unfortunately, models struggle to reproduce the Arctic halocline properly (Nguyen et al. 2009), and large temperature and salinity biases in the Arctic Ocean (Heuzé et al. 2023) make it difficult to properly define the halocline using the same criteria as in the observations. Manually deriving model-specific definitions is not ideal either, as the biases might vary over time. We, therefore, find that the uncertainty of properly defining the "correct" halocline in CMIP6 models based on Eq. (1) is too high and have chosen to investigate Arctic stratification in CMIP6 models using an indicator whose definition is less dependent on defining a halocline.

We therefore propose a new indicator of stratification strength, $\Delta\mathrm{PE}(H)$. First, we define the potential energy of the water column following Tailleux (2009) as

$$\mathrm{PE}(H) = \int_{H}^{\mathrm{surface}} g(z)\rho(z) z \, dz, \tag{3}$$

where H is a chosen depth level. We then look at the difference in potential energy between the simulated stratified water column and a fully mixed water column, which reflects the energy needed to fully mix the water column from the surface to a given depth:

$$\Delta\mathrm{PE}(H) = \mathrm{PE}(H) - \mathrm{PE}(H)_{\mathrm{mixed}}, \tag{4}$$

Here, $\mathrm{PE}(H)_{\mathrm{mixed}}$ is the potential energy of a completely mixed water column with a mean temperature and salinity down to depth H. The term $\Delta\mathrm{PE}(H)$ thus represents the potential energy stored in stratification, and as long as H is well below the typical halocline depth, APE and ΔPE should capture similar changes and be equally good indicators of stratification strength. However, $\Delta\mathrm{PE}(H)$ is preferred in models as its definition is independent of temperature and salinity gradients. Throughout the paper we will refer to ΔPE as stratification strength or potential energy stored in stratification. A comparison of APE and ΔPE is given in Fig. S3. We use $H = 300$ m (well below the halocline according to Heuzé et al. 2023), but have repeated the calculations with different values of H, and the qualitative results are not sensitive to this choice. We also note that ΔPE describes a process of irreversible mixing, whereas APE describes the difference to adiabatically rearranged minimum energy, which would be reversible.

3. Results

a. *Recent decades (1970–2014)*

1) Observed stratification changes

We start by analyzing hydrographic observations from four regions in the Arctic Ocean (Fig. 1); two in the AB (Beaufort Gyre and the Chukchi Sea) and two in the EB (Western and Eastern EB), consistent with previous studies (e.g., Polyakov et al. 2020a). The halocline base is deeper in the AB (~200 m) than in the EB (~90 m, Fig. 1). Since 1970 it has deepened in the AB (~7 m decade^{-1}) and shoaled in the EB (~3 m decade^{-1}), although the latter trend is not statistically significant. In the AB, the halocline freshens (~0.11 psu decade^{-1}), which other studies have documented (Carmack et al. 2016; Proshutinsky et al. 2019; Polyakov et al. 2020a). The EB halocline shows overall no statistically significant salinity trend, although a moderate salinification has been observed in the Eastern EB region in recent decades (Polyakov et al. 2020a, not shown here). The Eastern EB salinification and AB freshening were recently taken as indicators of the ongoing Atlantification and Pacification (Polyakov et al. 2020a), but we note that particularly Pacification is difficult to distinguish from the local freshening occurring in the upper Arctic Ocean due to increased runoff or precipitation. Alongside the halocline freshening in the AB, there is general warming (~0.04°C decade^{-1}) related to PW inflow (Polyakov et al. 2020a). Also in the EB the

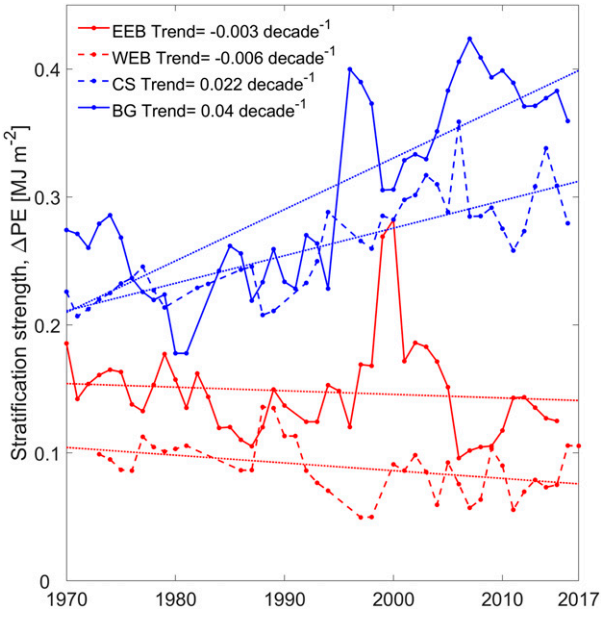

FIG. 2. Observed potential energy stored in stratification [ΔPE(H)] from 300 m following Eq. (4). Blue colors are used for the AB, and red colors are used for EB. WEB = Western Eurasian basin, EEB = Eastern Eurasian basin, CS = Chukchi Sea, and BG = Beaufort Gyre. All trends, except the EEB, are statistically significant.

halocline warms (~0.04°C decade^{-1}), but again, these trends are not statistically significant.

The contrasting changes in upper ocean salinity and temperature in the EB and AB result in different effects on the regional halocline stability and thus stratification. In Fig. 2, we present the observed regional time series of potential energy stored in stratification. There is a strong positive trend in ΔPE in the Chukchi Sea and Beaufort Gyre, which is associated with a strengthening of the stratification. In contrast, in the Western and Eastern EB, the ΔPE shows a negative long-term trend, meaning the stratification is weakened (although much weaker trends than in the AB and not statistically significant in the Eastern EB). These findings are consistent with Polyakov et al. (2018) who showed that the most considerable changes in Arctic Ocean stratification have occurred in the AB and other studies which show that the halocline has weakened in the EB toward the end of the twentieth century (Steele et al. 1989; Polyakov et al. 2017, 2020b). A comparison of ΔPE and APE, used in Polyakov et al. (2018) is shown in Fig. S3. Overall, the two metrics both show the opposite changes in the AB and EB, but ΔPE includes changes in the AW just below the halocline and therefore shows a stronger signal of Atlantification in the Western EB compared to APE, which only takes into account changes to the bottom of the halocline. Clearly, the trends are affected by how one chooses to represent stratification, and given their different definitions, the metrics also show significant differences in internal variability. In the following section, we compare the observed changes in stratification to simulations from 14 CMIP6 models.

2) SIMULATED STRATIFICATION CHANGES

In the AB, most models analyzed in this study are less stratified than observations (colors of bars in Fig. 3), as also discussed by Heuzé et al. (2023) and Khosravi et al. (2022). Notable exceptions are IPSL-CM6A-LR and NorESM2-LM. In the EB, most models are equally or more stratified than observations, with GFDL-CM4 and GISS-E2-1-H as exceptions. In general, the models do not correctly represent the difference in stratification between the two basins and instead have similar values throughout the whole Arctic (i.e., the same color of bars on all panels of Fig. 3)—a result consistent with the biases in water mass properties described in Heuzé et al. (2023) and Khosravi et al. (2022). In fact, several models are incorrectly more stratified in the EB than in the AB. However, the biases in stratification are not consistent throughout the Arctic and vary from region to region. It is worth noting that no model is too strongly biased to not be kept in this study, i.e., all stratification values are in the same order of magnitude as the observations.

In accordance with observations, all models show a positive trend in stratification (strengthening) in the AB over the period 1970–2014 (Fig. 3, length of the bars). However, the absolute values of the trends are much lower than in the observations. There appears to be no clear relationship between the mean strength of stratification and the magnitude of trends (not shown). The models also agree on a larger change in stratification in the AB compared to the EB, although they do not show the opposite trends between the basins. In the Western EB, almost all models simulate a strengthened stratification, and only CAMS-CSM1-0 produces a weakened stratification like the observations. In the Eastern EB, there is a larger disagreement among the models, both in the mean state and in their trends, and here two models (CanESM5 and EC-Earth3) simulate a weakened stratification. In summary, only three models indicate an Atlantification (as diagnosed through ΔPE) comparable to what has been observed. We emphasize here that we only investigate one ensemble member for each model, and that internal variability could have a significant impact on the trends during the 1970–2014 period where the external forcing is relatively weak. For example, experiments with a single model system (UKESM1-0-LL; not shown) show that among nine ensemble members, the trends in stratification in the Eastern EB (where the spread is largest) range between −0.0007 and +0.001 17 MJ m^{-2} yr^{-1}. In the next sections, we investigate how the trends are projected to continue or change into the future under a strong greenhouse-gas forcing scenario.

b. *Future trends in stratification*

The temporal anomalies of the simulated potential energy stored in stratification, ΔPE show significant variations in the various regions both in the historical period and under the ssp585 forcing scenario (Fig. 4). Within the EB, the models diverge regarding future stratification. Figure 4 shows large differences among the models, with the largest intermodel spread in the Eastern EB. Some models project a clear increase in EB stratification (e.g., GFDL-CM4, GFDL-ESM4,

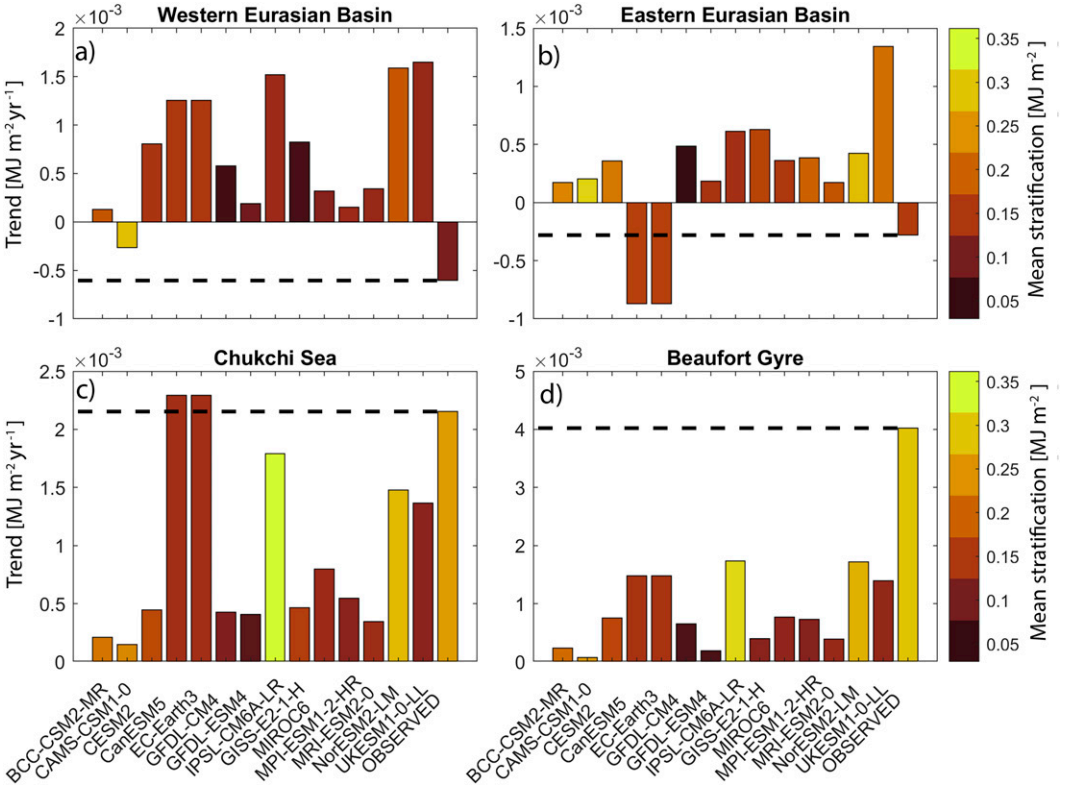

FIG. 3. Simulated trends in stratification strength, ΔPE, for each of the CMIP6 models listed in Table 1 from 1970 to 2014. Dashed black lines and rightmost bars indicate the observed trends (Fig. 2), and color bars indicate the mean stratification strength in different regions for each model. Note the different *y* axes on all panels.

GISS-E2-1-H, and CAMS-CSM1-0) while others project a clear decrease (e.g., UKESM1-0-LL, CanESM5, NorESM2-LM, and IPSL-CM6A-LR). The future weakening of the EB stratification was also shown by Lique et al. (2018) using the HiGEM model. Despite only two models showing an indication of Atlantification in the period 1970–2014, approximately half of the models predict a future weakening of the EB stratification and thus Atlantification. Despite the large spread in the EB, there is agreement among the models (except IPSL-CM6A-LR, plain yellow line) on an increased future stratification in the Chukchi Sea and Beaufort Gyre regions. This means that the observed strengthening of the halocline in the AB is projected to continue and amplify into the future. In the Beaufort Gyre, the trends continue throughout the twenty-first century, whereas in the Chukchi Sea, the curve flattens in the 2060s for many of the models, albeit with strong interannual variability. This is likely related to the fact that at this point the region is practically ice-free for large portions of the year, and the freshwater contribution from sea ice melt therefore decreases. The freshwater input from river runoff is expected to continue to increase, but due to the prevailing wind patterns in the region, most of this will accumulate in the Beaufort Gyre region and not stay in the Chukchi Sea region. The future trends in the AB are comparable to the observed trend in recent decades, but in the EB, both the trends and the interannual variations are amplified under the strong forcing scenario.

The spatial extent of future trends in stratification varies significantly among the selected models, but there are also some commonalities in the spatial patterns (Fig. 5). For example, there is a clear division and opposite trends in the AB and EB, similar to what has been documented by Polyakov et al. (2020a) and what can be seen from the lower right panel in Fig. 5. The opposing trends can be understood as the competing influences of the Atlantic and Arctic domains. All models show a weakening of stratification in some parts of the EB (red colors) and a strengthening of stratification in most parts of the AB (blue colors). However, the exact location, extent, and magnitude of the Atlantification signal varies, resulting in a large spread, especially in the Eastern EB. From Fig. 5 we see that some of the discrepancies shown in Fig. 4 are strongly related to the spatial extent of the signals and the use of fixed regions. Interestingly, for most models, the indicated Atlantification is mainly confined toward the Eastern parts of the EB and the Barents Sea outflow near the St. Anna trough and less toward Fram Strait. It is possible that because AW is in closer contact with sea ice north of Svalbard, more sea ice is melted there, resulting in increased surface freshening and hence a strengthening of the stratification. GISS-E2-1-H is the only model that

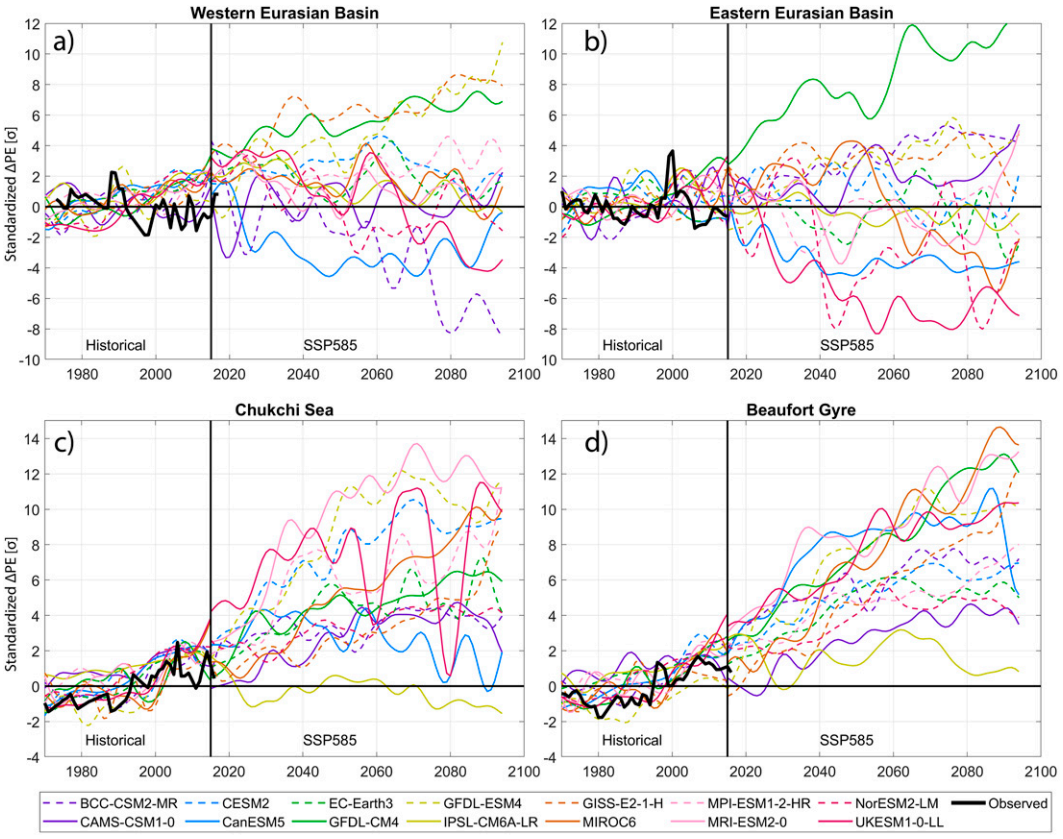

FIG. 4. Regional time series (standardized anomalies relative to 1970–2014 mean) of stratification strength, ΔPE (MJ m^{-2}), for the 14 CMIP6 models listed in Table 1. More positive values mean more energy is needed to mix the water column. All time series are low-pass filtered with a 5-yr cutoff frequency. Note the different *y* axes for the two basins. For comparison, the observed stratification over the period 1970–2017 is plotted in with thick black lines.

shows no indication of Atlantification, whereas IPSL-CM6A-LR, CanESM5, and UKESM1-0-LL show the largest spatial extent of Atlantic influence.

We quantify and summarize the historical and future trends for each region in Fig. 6. The dipole-like pattern is also clearly illustrated here, with obvious differences between the evolution of the EB and AB. The spread among the models is comparable in both basins (~3 MJ m^{-2} yr^{-1}), but this spread results in opposite signs in the EB, whereas, as shown previously, most models project an increase in stratification in the AB. Again, we note that some of these discrepancies reflect different spatial extent of the signals. The future trends in the AB are somewhat larger than the historical trends. More than half of the models show a strong weakening trend in the EB, with CanESM5, NorESM2-LM, IPSL-CM6A-LR, and UKESM1-0-LL having the largest changes. UKESM1-0-LL is an extreme in the Eastern EB with a trend 4 times stronger than any other model. These changes in stratification can be the result of changes in the upper ocean (SML and halocline) and water masses below the halocline, such as the AW. In the following section, we examine what drives the changes in stratification in the various regions and focus on the difference between the surface and AW layers.

c. *Atlantic water and surface trends*

We have now shown that the models diverge when predicting changes in stratification in the EB and show a large spread in the AB. Khosravi et al. (2022) noted that "model biases in the Arctic Ocean could have origins outside the Arctic Ocean and possibly in other components of the climate system. Identifying these origins in individual models is needed to improve the Arctic Ocean representation in CMIP simulations." To do so, we therefore focus on the water masses that are the primary drivers for stratification change: the surface waters and the AW. We assume that most changes at the surface are driven by local processes (e.g., sea ice melt/growth, river runoff, evaporation–precipitation, surface heat fluxes, etc.), and those in the AW layer are primarily advected in through the Fram Strait and the Barents Sea, and mainly related to processes beyond the boundaries of the Arctic Ocean. The question thus becomes: are the simulated changes in stratification mainly locally driven or remotely forced? Of course, the layers are not fully disconnected, and mixing occurs along the AW pathways, but Heuzé et al. (2023) revealed that in the CMIP6 models, there is a strong decoupling between the upper layer and the rest of the deep Arctic (below 200 m). This is partly attributed to an absence of ventilation, and as a

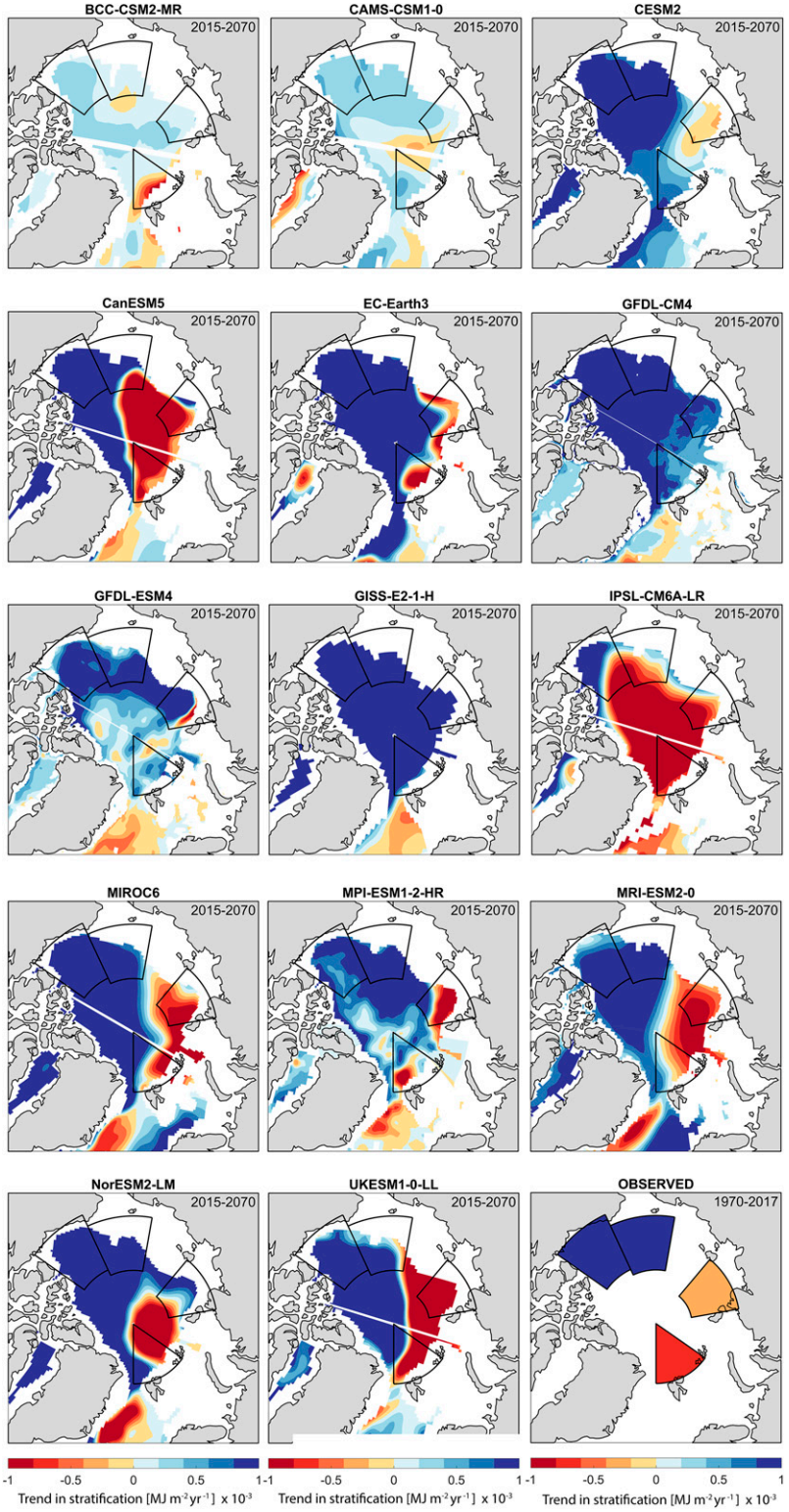

FIG. 5. Future spatial trends in stratification strength, ΔPE, under a strong greenhouse gas forcing scenario (ssp585) for the 14 CMIP6 models listed in Table 1. Negative values mean a weakening of stratification. All trends are annual means calculated over the period 2015–70. For comparison, the observed trends in stratification over the period 1970–2017 is plotted in the last panel.

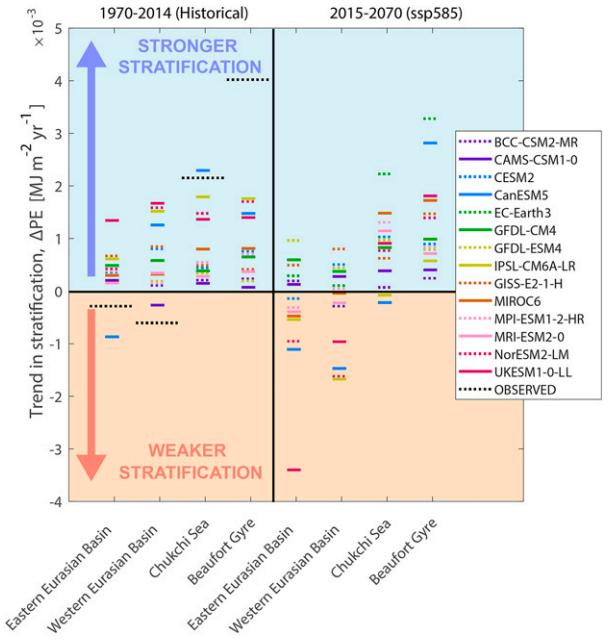

FIG. 6. Mean regional trends in stratification strength, ΔPE, for our 14 CMIP6 models. The trends over the historical period (1970–2014) are shown on the left, and the trends over the future period (2015–70) under a strong greenhouse-gas forcing scenario (ssp585) are shown on the right. As in Fig. 5, positive values (blue shading) denote increased stratification, and negative values (orange shading) denote weakened stratification. For comparison, the trends for the observations over the 1970–2017 period is shown by dashed black lines.

result, the properties of the Arctic AW layer are closely linked to the inflows.

We start by detailing the evolution of AW core temperature and salinity in the four different regions. As expected, with continued global warming, the AW temperature is projected to increase in all regions by all models (Fig. 7). Thick lines in Fig. 7 represent the multimodel mean anomalies relative to each model's historical mean, and colored envelopes indicate the minimum and maximum of the model spread per time step. A full overview of the property trends in the various models is presented in Table 2. We note that AW core properties are calculated based on each model's AW core depth (details in section 2c), which varies substantially from model to model (Heuzé et al. 2023). The models project an increase in AW temperature with a range of 0°–7°C relative to the historical mean toward the end of the twenty-first century. The AW temperature change is relatively linear over time and reaches a multimodel mean increase of 3.0°C in the EB and 2.5°C in the AB by 2100. Some models predict very weak trends in AW temperature (lowest in the EB = 0.013°C decade^{-1}), but the majority predict strong warming (highest in the EB = 0.740°C decade^{-1}), in accordance with what was shown by Khosravi et al. (2022). The average future AW temperature trend in the EB is 0.33°C decade^{-1}, compared to an observed trend of 0.06°C decade^{-1} from 1970 to 2017. Less intuitive, perhaps, is the future change of AW salinity. Most models simulate a freshening of the AW layer throughout the Arctic (Table 2), except EC-Earth3 which simulates an increase in AW salinity in all regions. Averaged across the regions, the multimodel mean freshening is approximately 0.5 psu by the end of the century, as also shown by Khosravi et al. (2022).

The decrease in AW salinity indicates that the northward freshwater flux through the Fram Strait and Barents Sea Opening increases, which is consistent with results from Zanowski et al. (2021). Over 2015–70 all models, except CAMS-CSM1-0 and GFDL-CM4, show a positive trend in the liquid freshwater flux through the Barents Sea opening, which mainly consists of northward-flowing AW (Fig. S4b). The freshwater flux through Fram Strait is more complex, as it consists of both a southward and a northward flow. Here we observe a negative trend in the (northward) freshwater flux (Fig. S4a), meaning an increase in the net southward freshwater flux. This makes sense, as the increase in the outflowing freshwater is larger than the increase in the inflowing freshwater (as it also includes the other freshwater sources). All in all, a decrease in the northward-flowing AW contributes to a freshening at intermediate depths and ultimately an increase in the total freshwater content of the Arctic and the southward export of freshwater, as also shown by Zanowski et al. (2021). Our findings stress an important point that has not been stated in current literature, namely that the future freshening of the Arctic Ocean may be attributed to both surface and AW changes. Since there is a strong decoupling between the upper layer and the rest of the deep Arctic in these models, and the AW properties are strongly related to the AW inflow properties (Heuzé et al. 2023), we speculate that the Arctic freshening is partly remotely driven.

It is important to remember that it is not only the water mass properties but also the depth and thickness of the various layers that can affect changes in stratification. We do not detail biases and changes in AW core depth but refer the readers to Heuzé et al. (2023) and Khosravi et al. (2022), and note that the effects of these changes are integrated in the ΔPE metric. As we continue with the temperature and salinity evolution of the surface layer (0–50 m), different model behaviors become even more evident (Table S1). In the AB, all models project a freshening and warming of the surface layer, consistent with current observations [Table S1 and Solomon et al. (2021)] and the expected continuation of AB freshening (Haine 2020). Averaged across the models, the absolute change in surface salinity is expected to reach approximately −1.5 psu by the end of the century (Fig. S5). In the EB, on the other hand, many models project a freshening, but some project a surface salinification (Fig. S5). Some of the models that project a surface salinification are the same that project an AW salinification, but for others, there are opposite trends in the AW and surface layers. There is no consistent relationship between the direction of surface trends and trends in the AW layer, and there is also no clear relationship between changes in AW/surface properties and freshwater/salinity fluxes through the Fram Strait and the Barents Sea (not shown). The multimodel mean still projects a freshening in both the Eastern and Western EB, although some models have

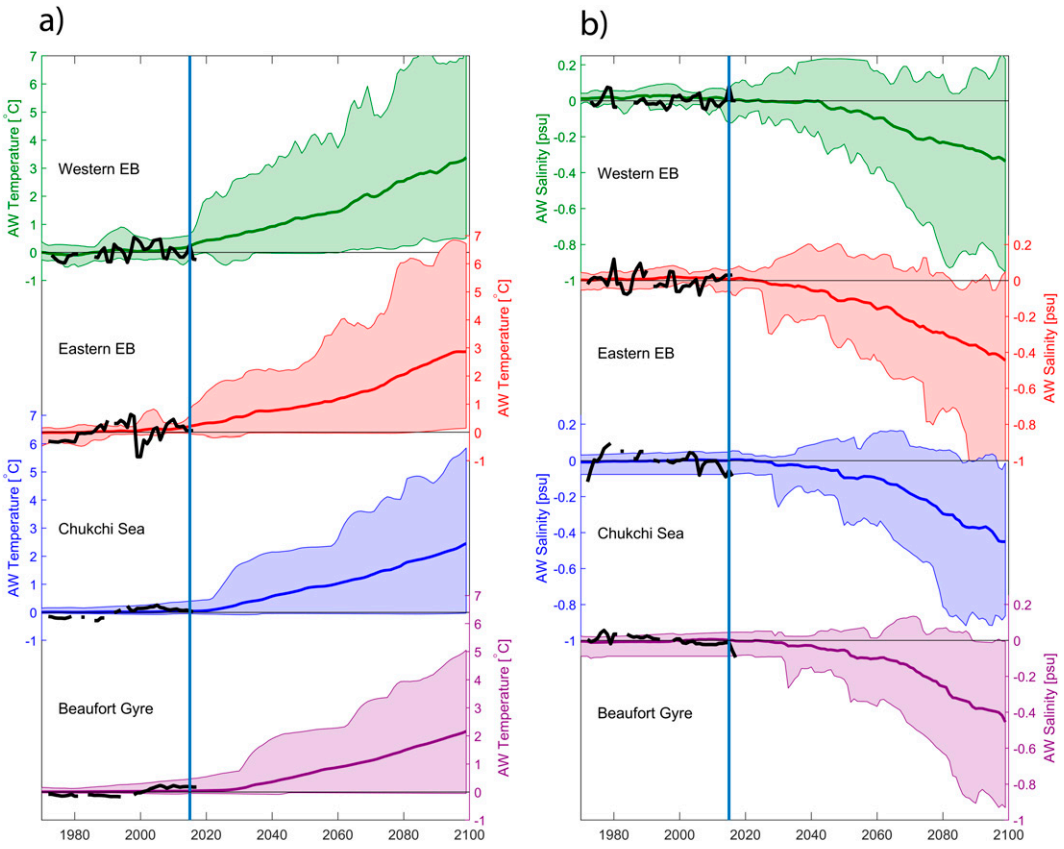

FIG. 7. Regional time series of normalized (reduced to anomalies relative to 1970–2014 model mean) (a) Atlantic Water core temperature and (b) Atlantic Water core salinity from the CMIP6 models listed in Table 1. Thick lines represent the multimodel mean, and envelopes show the minimum and maximum of the model spread per time step. For comparison, the AW core anomalies from the observations over the 1970–2017 period are shown by black lines. The Atlantic Water core properties are calculated as the properties at the temperature maximum below 100 m.

opposing trends. Figures 7 and S5 emphasize the importance of the regional aspect when investigating future Arctic Ocean change, and thus provides further detail than the basin-wide averages provided by Khosravi et al. (2022). Even though the general change is similar (AW warming and freshening), the regions are projected to evolve somewhat differently or on different time scales. For example, the Eastern and Western EB are exposed to different processes as they have a different seasonal ice cover, which is projected to change differently in the future (Notz and SIMIP Community 2020). Taking an EB or AB mean, as is common practice in CMIP studies of the Arctic Ocean, is therefore not ideal since one might lose important information and average out important regional differences. The different evolution in surface properties evident from Fig. S5 and Table S1 also stresses the importance of studying models individually and not as a multimodel means. These results give an indication to the origin of biases in stratification, because differences in salinity and temperature trends result in different contributions to the overall density profile.

Figure 8 shows the comparison of density changes in the upper ocean (0–50 m; lower per panel) and at intermediate depth below the halocline (150–500 m; lower panel) for each model in the western EB and the Beaufort Gyre regions (the Eastern EB and Chukchi regions are shown in Fig. S6). Red and blue bars denote the relative contributions of temperature and salinity trends to the total density trends (fat gray bars), respectively. Note the different scales on the *y* axis. In the upper ocean, the density changes are mainly driven by salinity changes. In contrast, at intermediate depth, the density changes are more equally attributed to both temperature and salinity. In some cases, temperature and salinity have opposite effects (EC-Earth3 and UKESM1-0-LL), and the contribution from warming is slightly larger than the salinification, resulting in an overall decrease in AW density. In other cases, for example in CAMS-CSM1-0, salinification overpowers the warming. In general, the upper ocean density trends are much larger than the trends at intermediate depth. Opposing results in the EB stratification are primarily related to opposite changes in surface density (Fig. 8a). However, density trends further down in the water column also contribute and may either enhance or diminish the impact of the surface trend on the overall stratification. For example, in the Western EB, changes in the surface and AW layer in CanESM5 contribute to a weakening of the stratification. In CESM2, on the other

TABLE 2. Future Atlantic Water core (temperature maximum below 100 m) temperature and salinity trends for each of the CMIP6 models (forcing scenario ssp585) over 2015–70. For comparison, the last row indicates the trends for the observations over the 1970–2017 period. All values are given in °C decade^{-1} and psu decade^{-1}. Statistically nonsignificant trends ($p \geq 0.05$) are shown in italic.

	Western EB		Eastern EB		Chukchi Sea		Beaufort Gyre	
	θ	S	θ	S	θ	S	θ	S
BCC-CSM2-MR	0.013 ± 0.004	−0.016 ± 0.005	−0.002 ± 0.000	0.003 ± 0.001	−0.002 ± 0.000	−0.004 ± 0.000	−0.003 ± 0.000	−0.004 ± 0.000
CAMS-CSM1-0	0.032 ± 0.008	0.015 ± 0.002	0.012 ± 0.001	−0.005 ± 0.001	*0.001 ± 0.001*	−0.015 ± 0.001	0.006 ± 0.001	−0.008 ± 0.002
CESM2	0.355 ± 0.018	−0.062 ± 0.007	0.310 ± 0.013	−0.047 ± 0.005	0.224 ± 0.012	−0.043 ± 0.002	0.115 ± 0.010	−0.045 ± 0.002
CanESM5	0.729 ± 0.026	−0.036 ± 0.004	0.428 ± 0.021	−0.082 ± 0.006	0.454 ± 0.029	−0.040 ± 0.006	0.525 ± 0.029	−0.017 ± 0.004
EC-Earth3	0.606 ± 0.024	0.028 ± 0.004	0.470 ± 0.013	0.011 ± 0.005	0.429 ± 0.031	0.056 ± 0.003	0.225 ± 0.033	0.041 ± 0.004
GFDL-CM4	0.143 ± 0.005	−0.021 ± 0.001	0.120 ± 0.005	−0.020 ± 0.002	0.176 ± 0.010	−0.009 ± 0.001	0.088 ± 0.007	−0.008 ± 0.001
GFDL-ESM4	0.097 ± 0.018	−0.032 ± 0.002	0.152 ± 0.009	−0.026 ± 0.001	0.121 ± 0.008	−0.024 ± 0.001	0.061 ± 0.005	−0.005 ± 0.001
IPSL-CM6A-LR	0.402 ± 0.023	*−0.004 ± 0.005*	0.301 ± 0.021	−0.018 ± 0.006	0.330 ± 0.028	*−0.012 ± 0.007*	0.360 ± 0.023	−0.020 ± 0.007
GISS-E2-1-H	0.040 ± 0.007	*0.004 ± 0.007*	0. 155 ± 0.008	*0.000 ± 0.005*	0.155 ± 0.002	−0.009 ± 0.002	0.125 ± 0.005	−0.009 ± 0.002
MIROC6	0.286 ± 0.019	−0.092 ± 0.003	0.122 ± 0.014	−0.091 ± 0.003	0.162 ± 0.004	−0.072 ± 0.003	0.144 ± 0.004	−0.063 ± 0.004
MPI-ESM1-2-HR	0.314 ± 0.016	−0.015 ± 0.002	0.105 ± 0.016	−0.038 ± 0.002	0.242 ± 0.019	−0.016 ± 0.001	0.301 ± 0.014	−0.009 ± 0.001
MRI-ESM2-0	0.444 ± 0.012	−0.094 ± 0.004	0.291 ± 0.013	−0.093 ± 0.003	0.268 ± 0.015	−0.100 ± 0.003	0.207 ± 0.016	−0.092 ± 0.005
NorESM2-LM	0.346 ± 0.017	−0.063 ± 0.005	0.171 ± 0.024	−0.118 ± 0.005	0.312 ± 0.020	−0.096 ± 0.004	0.299 ± 0.022	−0.090 ± 0.005
UKESM1-0-LL	0.740 ± 0.028	*−0.009 ± 0.005*	0.713 ± 0.024	−0.038 ± 0.008	0.735 ± 0.024	−0.030 ± 0.008	0.604 ± 0.036	−0.035 ± 0.006
OBSERVED	0.062 ± 0.030	*−.0001 ± 0.004*	0.100 ± 0.034	*−0.000 ± 0.005*	0.087 ± 0.012	−0.018 ± 0.005	0.086 ± 0.008	−0.014 ± 0.002

hand, the surface trends contribute to a strengthening of the stratification, and the intermediate layers contribute to a weakening of the stratification. In summary, the relative change between the upper ocean and intermediate layer ultimately determines whether the density gradient increases or decreases. We detail these vertical density gradients and how they change over time in the following section.

d. Future density gradients

We compare two models, GFDL-CM4 and NorESM2-LM, which project distinctly opposite changes in stratification in the EB (Fig. 6). In Fig. 9 we present the temporal development of temperature and salinity profiles for the GFDL-CM4 model, which projects a strengthening in stratification in all regions. Profiles shown in Figs. 9b and 9d represent the linear trends in temperature and salinity at each depth level over 2015–70. The temperatures are projected to increase throughout the whole water column, but the change is largest between 200 and 500 m and smallest in the halocline, just below the surface mixed layer. These trend profiles might not solely be due to a change in properties at the given depths but are also a result of the upward or downward movement of the AW and/or a deepening or shoaling of the SML. Due to space limitations, we do not investigate these changes in this paper, but Khosravi et al. (2022) give a good overview of changes in AW core depth and changes in SML depth.

The salinity trend profiles (Fig. 9d) show the largest trends at the surface, which gradually decreases with depth. In this model, below 300 m, there is almost no change in salinity, despite a small positive trend in AW salinity in the AB regions. This is thus an example of a model where upper ocean salinity changes primarily drive the stratification changes. These projections appear plausible, and we can relate the changes to known mechanisms. However, this is a good example of why it is dangerous to conclude future Arctic Ocean changes based on a single model system: A study based on a different model system may provide an opposite result. Figure 10 shows the temperature and salinity trend profiles for NorESM2-LM, a model that shows a weakening of the stratification in the EB and a strengthening of stratification in the AB. Overall, the vertical distribution of temperature trends looks very similar between NorESM2-LM and GFDL-CM4, which is true for all other models (not shown). Although the absolute values (and mean states) vary from model to model, they all simulate a positive temperature trend throughout the whole water column, with a maximum around 200-m depth and a minimum just below the SML. However, the salinity trends are very different. In NorESM2-LM (and several other models), there are significant salinity trends throughout the whole water column. In NorESM2-LM, the AW salinity decreases in all regions, especially after 2040, contributing to the weakening of the stratification. In the AB regions, this is balanced by a stronger freshening of the surface, but in the western EB, the surface is getting saltier, meaning that both the AW layer and the surface layer contribute to a weakening of the density gradient. Figure 11 shows the trend in density at

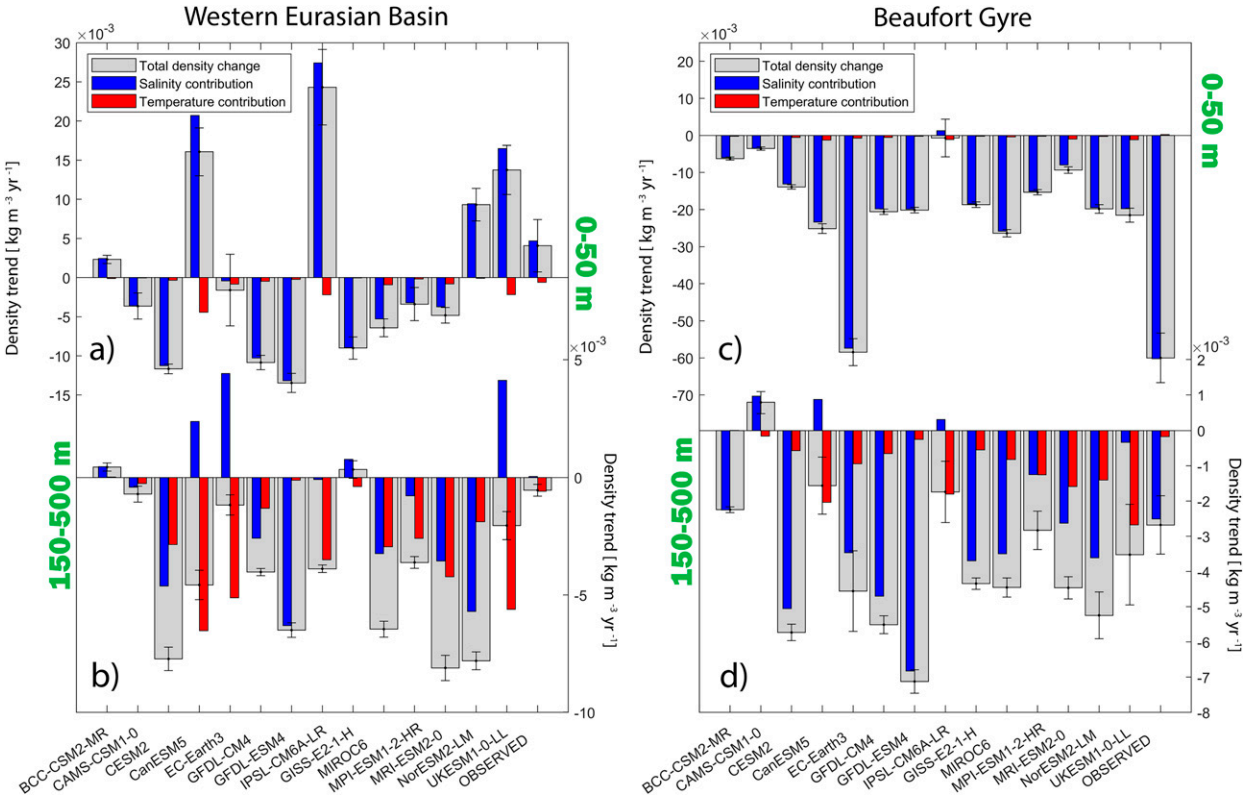

FIG. 8. Trends (2015–70) in density (a),(c) in the upper ocean and (b),(d) at intermediate depth for the (left) Western Eurasian basin and (right) Beaufort Gyre region for each of the CMIP6 models listed in Table 1. Red and blue bars denote the relative contributions of temperature and salinity trends to the total density trends (thick gray bars). Positive values mean increased density, and negative values mean decreased density. For comparison, the trends from the observations over the 1970–2017 period are shown in the last column.

each depth level over 2015–70 for the two models. The combined effects of temperature and salinity yield an overall decrease in density throughout the whole upper 800 m of the water column for these two models. In GFDL-CM4, the profiles look similar for all four regions, with the largest decrease in the upper ocean and gradually decreasing trends with depth, increasing the gradient between the upper and intermediate layers. In NorESM2-LM, the profiles in the AB look similar, but in the EB regions, the (negative) density trend increases with depth in the upper 200 m (red box, Fig. 11), resulting in a decreased density gradient there. The density trend profiles provide a nice way to compare the hydrographic changes with depth in the various regions and highlight how differently the hydrographic structure is transformed in the multiple models under a similar climatic forcing. The density trend profiles for all models are shown in Fig. 12.

In the EB, most models agree on a negative density trend below 200 m, but above they diverge. Here we also see large discrepancies in how quickly the density trends increase or decrease with depth, thus the extent of the water column that is changed. Again, this is related to the SML depth, which varies and changes differently over time (Fig. 12). In the Beaufort Gyre region, the models have a very similar shape, but already in the Chukchi Sea, we see that models start to diverge, with some projecting densification of the water column and some projecting a negative trend in density throughout the water column. To summarize, there are many reasons why the models diverge on future stratification in the EB—the divergence is partly related due to different/opposite trends at the surface and partly due to a different balance between the strength of density trends at the surface and at AW depth, or both.

e. *Atlantification in the future*

Under the ssp585 strong greenhouse gas forcing scenario, there is good agreement among the models that the Arctic Ocean will continue to warm into the future with the largest warming in the AW layer and the EB. Accompanying this warming is a northward shift of ecosystems (Polyakov et al. 2020a, and references therein), a diminishing sea ice cover (Notz and SIMIP Community 2020), and further changes that we can combine under the term Atlantification, as parts of the Arctic Ocean gradually become more similar to the North Atlantic. However, it is not given whether Atlantification will continue to be a metonymy for "weakening in stratification"—its primary manifestation in the EB in recent decades (Polyakov et al. 2017).

The implications of changing stratification are numerous. As highlighted by Polyakov et al. (2020a), it can affect vertical

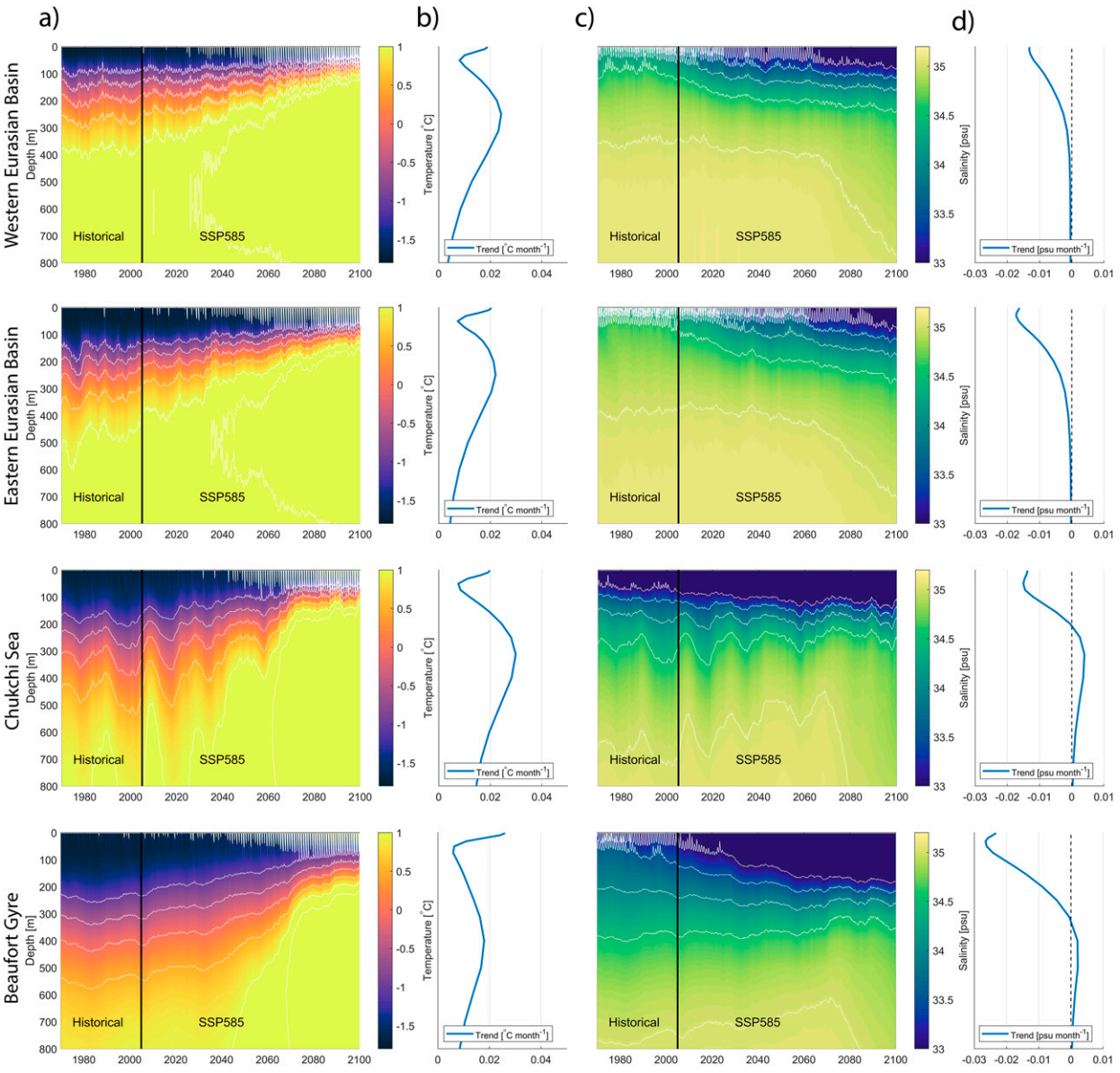

FIG. 9. Monthly mean upper ocean (a) temperature and (c) salinity from GFDL-CM4 from 1970 to 2100 for each region identified in Fig. 1. Linear trends are calculated for each depth level from 2015 to 2070 for (b) temperature and (d) salinity.

fluxes of nutrients and dissolved gasses and hence impact biology, but it mainly affects the vertical distribution of heat and hence the sea ice cover. Khosravi et al. (2022) also mention the potential impact of model biases on the simulated sea ice cover. We, therefore, investigate whether there is a relationship between the diverging stratification trends and the rate of sea ice decline in the EB. We now focus on the trends in the first half of the future scenario (2015–45) where there is still sea ice left in the EB. The top panels of Fig. 13 show the future "degree" of Atlantification (here arranged in order of decreasing stratification trend) for the different models in the EB. Models projecting the strongest weakening of stratification are found toward the left and those projecting the strongest increase in stratification are found toward the right. Similarly to Fig. 6, CanESM5, UKESM1-0-LL, EC-Earth3, and MPI-ESM1-2-HR are the models with the strongest degree of future Atlantification in both the Western and Eastern EB. IPSL-CM6A-LR also shows strong Atlantification in the Western EB and NorESM2-LM also shows strong Atlantification in the Eastern EB. In contrast, GFDL-CM4, GFDL-ESM4 and GISS-E2-1-H have the smallest degree of future Atlantification as they project an increase in stratification in both regions. The lower panels in Fig. 13 show the trends in winter (March) sea ice volume in these regions following the same order as the panels above. From these figures we see that the models with strongest degree of Atlantification (i.e., weakened stratification)

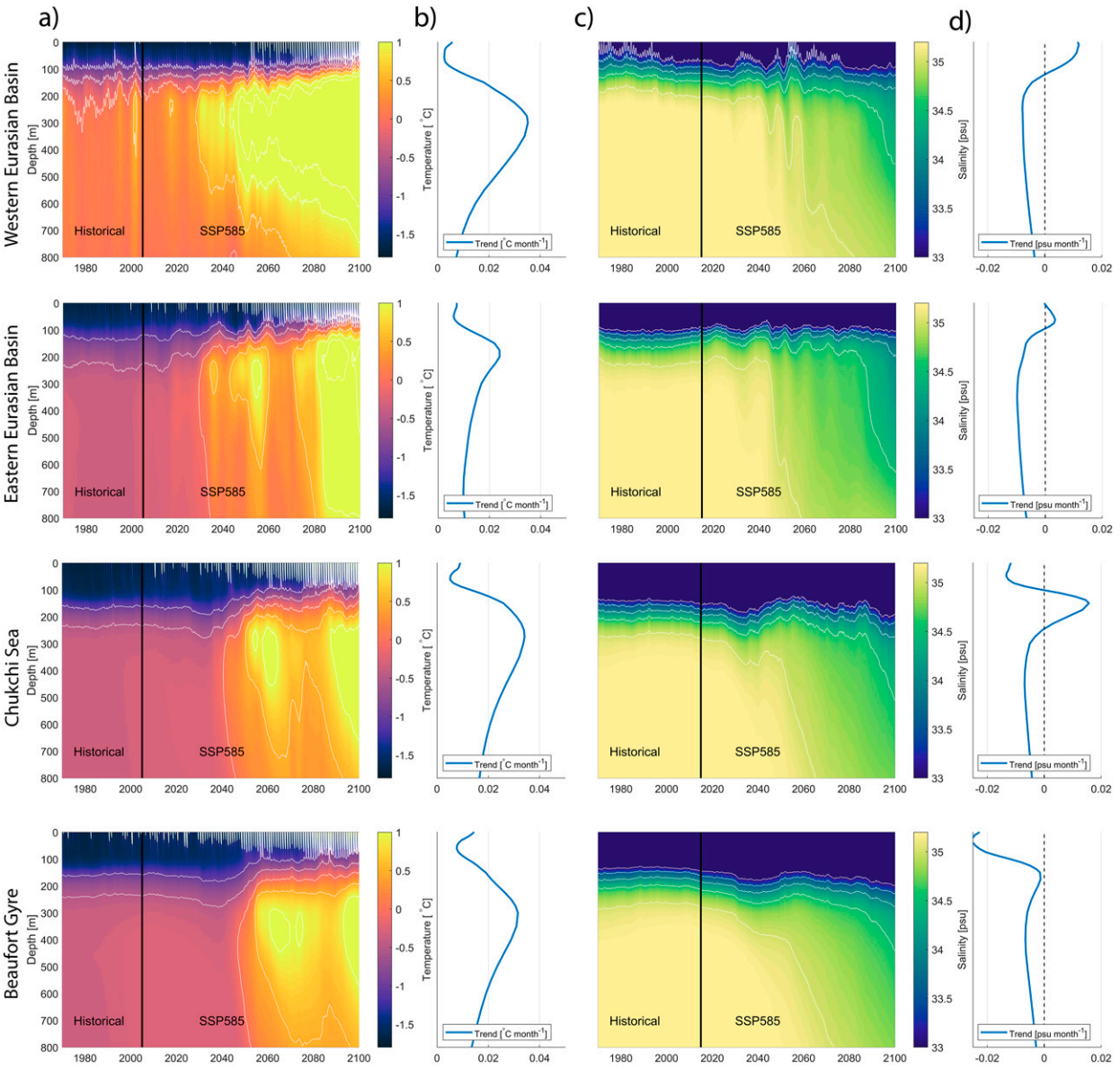

FIG. 10. Monthly mean upper ocean (a) temperature and (c) salinity from NorESM2-LM from 1970 to 2100 for each region identified in Fig. 1. Linear trends are calculated for each depth level from 2015 to 2070 for (b) temperature and (d) salinity.

project the strongest decline in sea ice in these parts of the EB. This is not surprising; although there are many factors influencing the sea ice trend, the ocean plays an increasingly important role, especially in the EB (Carmack et al. 2015). Our results show an across-model correlation of $r = 0.64$ between the sea ice volume trends and stratification trends in the Western EB and an across-model correlation of $r = 0.76$ in the Eastern EB (statistically significant at 95% level). The relationship is not perfect, and this is likely related to the mean sea ice state of the models or other important processes. For example, MPI-ESM1-2-HR has a very weak decline in sea ice volume compared to its strong degree of Atlantification in the Eastern EB, but since it finished the historical run with a low sea ice thickness compared to the other models (not shown), it simply cannot have a large volume trend. For reference we have therefore provided a table of mean sea ice volume at the beginning and in the middle of the ssp585 scenario (Table S2). Although correlation does not imply causation, there appears to be some relationship or commonality among the models that have a faster decline of sea ice and a weakening of stratification in the EB.

Since the models are roughly equally divided among two different stratification scenarios, it is unclear whether the currently ongoing weakening of the stratification in the EB will continue or not. Following Heuzé et al. (2023) and Khosravi et al. (2022), there is no clear evidence of certain models being significantly better at accurately reproducing the Arctic Ocean

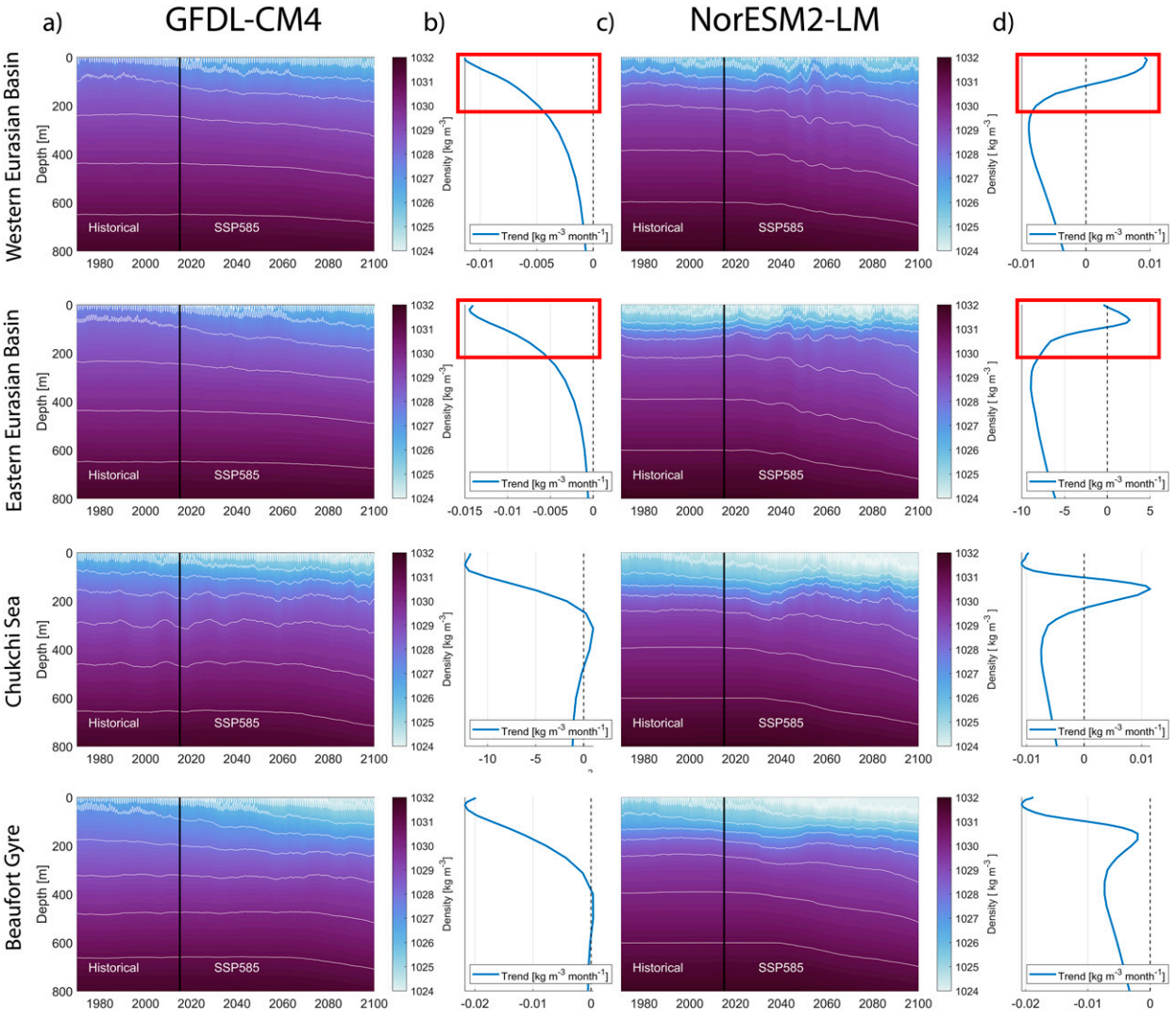

FIG. 11. Monthly mean upper ocean density from (a) GFDL-CM4 and (c) NorESM2-LM from 1960 to 2100 for the regions identified in Fig. 1. Linear trends are calculated for each depth level from 2015 to 2070 for (b) GFDL-CM4 and (d) NorESM2-LM. Red boxes indicate the depth interval in the Western EB and Eastern EB regions where the slope of the density trend profile is opposite for the two models, resulting in opposite changes to the stratification.

hydrography and circulation, and we can therefore not favor certain models or either of the scenarios. There is also no clear relationship between models with higher or lower resolution. As suggested by our companion paper, Heuzé et al. (2023), improvements could focus on ventilation, dense water overflows and inflow properties. There are also large biases in AW flow speed and patterns, and most CMIP6 models show a strong decoupling between the upper layers and the rest of the deep Arctic not consistent with observations.

4. Discussion and conclusions

This study quantified recent and future trends in upper Arctic Ocean stratification, temperature, and salinity in an ensemble of 14 CMIP6 models and compared these to a unique dataset of hydrographic observations dating back to 1970. In agreement with observations (e.g., Polyakov et al. 2020a), the models simulate a freshening and warming of the upper Amerasian basin (AB) and large parts of the Eurasian Basin (EB) over the period 1970–2014. These changes are associated with a general strengthening of the stratification, but there is a large spread among the simulated trends and mean stratifications. Although only three out of the 14 models simulate a weakening of the stratification in the EB that is comparable to observations, all models indicate different trends in stratification in the AB and EB. We note that for the 1970–2014 period, forcing is modest and internal variability likely influences these trends.

Because of temperature, salinity, and stratification biases in CMIP models, simulating and defining the halocline in models is challenging, especially when studying it in a suite of models

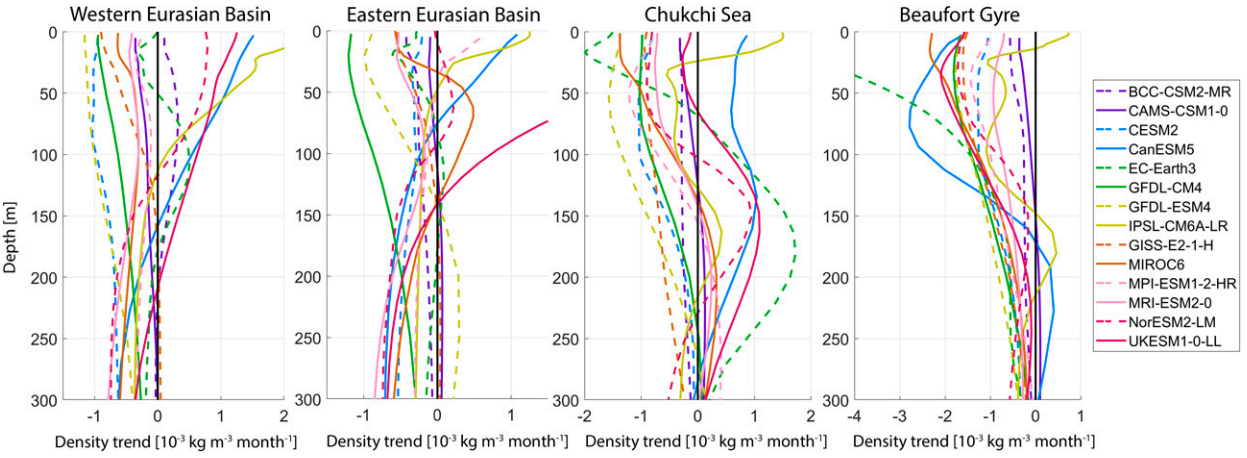

FIG. 12. Regional vertical profiles of the linear trend in density (similar to Figs. 11b,d) over the period 2015–70 from the CMIP6 models listed in Table 1. A stronger (negative) trend near the surface (~0–100 m) compared to intermediate depths (~150–300 m) results in a strengthened stratification. Note the different x axis for each panel.

under a climate change scenario. To compare and evaluate simulated Arctic stratification meaningfully, we, therefore, proposed a new indicator of stratification, ΔPE. This is an integral of the potential energy needed to fully mix the water column from the surface down to 300-m depth. Typical Arctic Ocean values are about 0.1 MJ m^{-2}, but the Beaufort Gyre and the Chukchi Sea have twice as strong stratification. Temporal change and regional contrasts observed by more

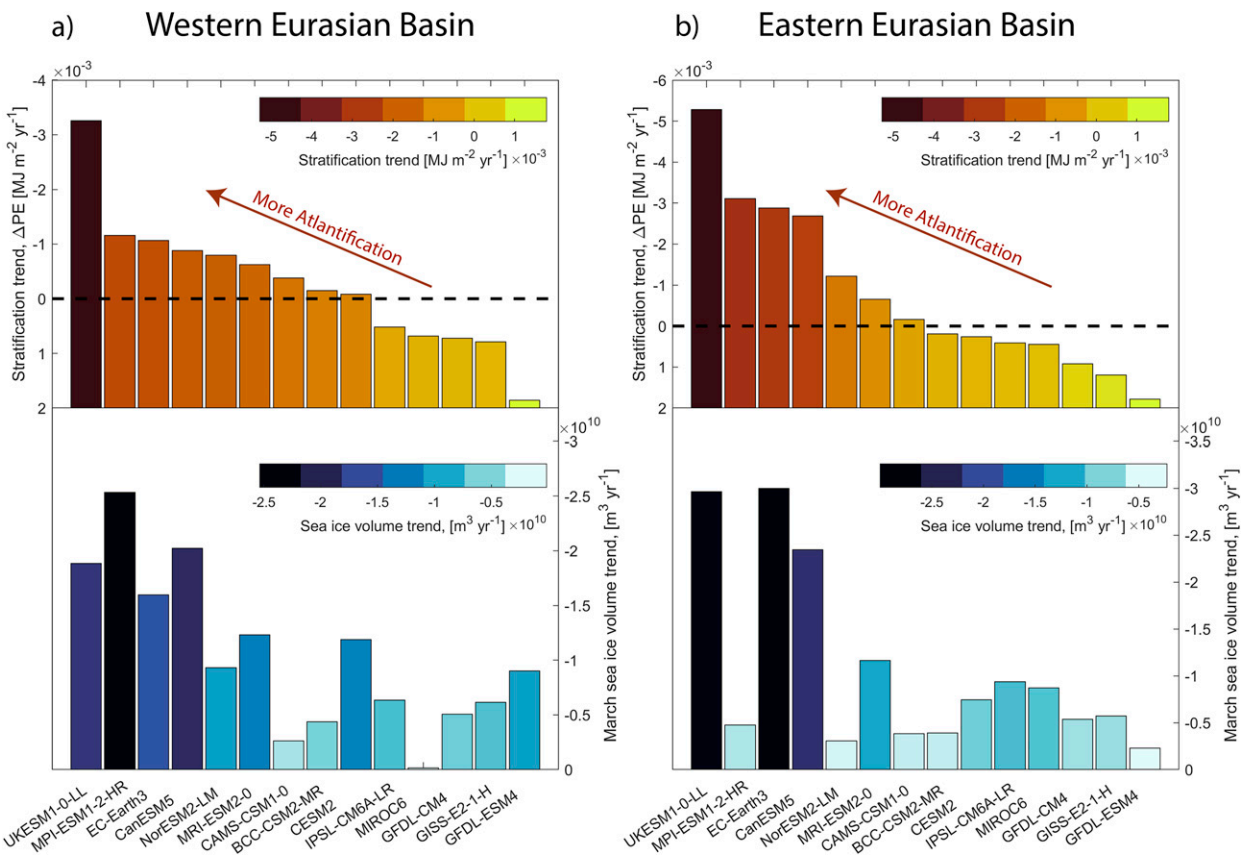

FIG. 13. (top) "Degree" of future Atlantification in the (a) Western and (b) Eastern Eurasian basin, defined by trends in ΔPE (2015–45). The models are arranged in order of decreasing stratification trend, with models projecting the strongest weakening of stratification toward the left and strongest increase in stratification toward the right. (bottom) Trends in winter (March) sea ice volume (2015–45) for each of the models, following the same order as the panels above. The length of the bars and their colors indicate the same values.

traditional stratification definitions (e.g., Polyakov et al. 2020a) are captured well by this new parameter, whose definition is not sensitive to model biases.

There is a reassuring across-model agreement within the Beaufort Gyre and the Chukchi Sea for near-surface stratification. Here the upper ocean layer will become fresher (on average 0.18 psu decade^{-1}), warmer (on average 0.35°C decade^{-1}) and more stratified in the future (on average 1.1×10^{-4} MJ m^{-2} decade^{-1}), but there is a large spread in the magnitude (likely due to different freshwater input and differences in the freshwater pathways). There is also simulated future warming (0.24°C decade^{-1}) and freshening (−0.03 psu decade^{-1}) occurring further down in the Atlantic Water (AW) layer. The entire water column is therefore getting less dense, but the surface freshening is so strong that the stratification is overall increasing in these regions. We did not examine the detailed causes of the future surface freshening but hold it as likely that both redistribution and local melting of sea ice, increased river runoff, increased glacial melt, and increased freshwater inflow through Bering Strait will all contribute significantly—as they do today (Haine et al. 2015; Haine 2020; Solomon et al. 2021). Throughout the upper Arctic Ocean, density trends are dominated by changes in salinity, but at intermediate depth, temperature and salinity changes contribute equally to the density trends.

In both the Eastern and Western EB, there is a divergence between the models regarding future stratification. Approximately half of the models project a strengthening of stratification here, and the other half project the opposite. The divergence is partly caused by opposing trends in upper ocean temperature and salinity. Additionally, the divergence is related to different spatial extent of the Atlantification and Pacification signals, not captured in the analysis due to the use of fixed regions. Furthermore, we discuss how the differences in stratification are related to different balances between trends in the upper ocean and trends at intermediate depths. Across the suite of models, there is a warming of the EB AW layer, but it varies between 0° and 7°C toward the end of the century. A majority of the models also project a freshening of the EB AW layer (0–0.9 psu), starting approximately in the 2050s. The AW warming and freshening result in a reduced density at intermediate depths, weakening the stratification. In about half of the models, these changes are counterbalanced by an upper-ocean freshening resulting in a strengthened stratification also in the EB. However, in some models, parts of the EB upper ocean experience a salinification, or the AW density change dominates (or both), aiding to an overall weakened stratification. It is difficult to judge which of the two stratification scenarios is the most likely. The divergence appears to impact the projections of sea ice, and we report on an across-model correlations ($r = 0.64$ and $r = 0.76$) between the trends in sea ice volume and trends in stratification. The models that project a weakened stratification in the EB also project a stronger decline in sea ice volume here.

In summary, observations and simulations agree that the Arctic Ocean is becoming warmer and that there is ongoing freshening in the AB. The simulations also agree that the observed weakening of the stratification in the EB does not spread eastward into the AB. The warming is unsurprising on a globally warming planet, and the future warming of the AW layer is most pronounced. In that regard, it is consistent with using the term Atlantification, as these waters are becoming more similar to those farther south. However, it is unclear whether Atlantification will continue to be analogous to a weakening in stratification. Of the models we analyzed, half of the models predicted a strengthening of the EB stratification. This is not what is currently associated with Atlantification. Further work is thus required before we can have more confidence in the future development of the EB. First, we need to improve the model's capability to simulate Arctic hydrography. Particular emphasis should be on the representation of AW circulation, ventilation, and the connections between the shelves and the deep basins (Heuzé et al. 2023). Additionally, there is an urgent need for more multiscale (in time and space) observational campaigns, such as the recent MOSAiC expedition (Rabe et al. 2022), that simultaneously provide in situ data of all the components of the Arctic climate system. Such campaigns result in a better understanding of specific processes and their interaction, which then can be used to improve their representation in the models. Long-term mooring deployments in the central Arctic are also needed to understand the variability at various time scales.

Our study highlights the importance of a multimodel approach for studies of the future Arctic Ocean. Given the relatively large biases and opposite trends, relying on a single or just a few model systems is insufficient and may result in misleading conclusions. However, it is important to analyze and interpret the models individually, not as a multimodel mean. Our results clearly show that averaging (opposite) model trends and properties will yield results that seem credible but are completely nonphysical. This is particularly important for profiles, as water masses are distributed differently in the vertical, and the same processes, therefore, have an effect at different depths. Thus, an important takeaway from this study is that we strongly discourage using multimodel averages to investigate trends in Arctic hydrography. Also, many ensembles from a single model system may skew the results toward specific model biases created by physical or thermodynamical deficiencies. However, studies using many ensembles could give important information about the relative importance of internal variability compared to external forcing, and we stress the need for such analysis. Clearly, studies of the Arctic Ocean should be based on and validated by observations due to the inherent large local uncertainty of the models.

Acknowledgments. Morven Muilwijk received funding for this work from the European Union's Horizon 2020 research and innovation programme under Grant Agreement 101003826 via project CRiceS (Climate Relevant interactions and feedbacks: the key role of sea ice and Snow in the polar and global climate system) and from the University of Bergen, Bjerknes Center for Climate Research. Aleksi Nummelin received funding for this work from Research Council of Norway project KeyClim (295046). Igor

V. Polyakov acknowledges support from the United States NSF grants (AON-1724523, AON-1947162) and ONR grant (N00014-21-1-2577). Céline Heuzé received funding for this work from Vetenskapsrådet under Grant Agreement 2018-03859. Support for Hannah Zanowski was provided by the Office of the Vice Chancellor for Research and Graduate Education at the University of Wisconsin–Madison with funding from the Wisconsin Alumni Research Foundation. Lars H. Smedsrud was supported by the Norwegian Research Council through the Nansen Legacy Project (Grant 276730). The authors acknowledge the World Climate Research Programme, which, through its Working Group on Coupled Modelling, coordinated and promoted CMIP6. The authors also thank the various modeling groups for producing and making their model output available, the Earth Grid System Federation (ESGF) for archiving and providing access, and the multiple funding agencies that support CMIP6 and ESGF. Computing and storage resources were provided by Sigma2, the National Infrastructure for High-Performance Computing and Data Storage in Norway, and the authors thank Michael Schulz, Yanchun He, and Richard Davy for coordinating the local storage of CMIP6 data and Anaïs Bretones for support with the data download. The authors would also like to thank those who went to sea and collected valuable observations in harsh Arctic conditions over the last century. Finally, we thank Erica Rosenblum and two anonymous reviewers, as well as the editor Laure Zanna, for their many comments that greatly improved this manuscript.

Data availability statement. CMIP6 data are freely available via the Earth Grid System Federation. For the analysis presented here, we used the Geophysical Fluid Dynamics Laboratory (GFDL) node: https://esgdata.gfdl.noaa.gov/search/cmip6-gfdl/ and the Lawrence Livermore National Laboratory node: https://esgf-node.llnl.gov/projects/cmip6/. Annual mean temperature and salinity profiles over the historical period (1970–2017) from the observations and CMIP6 models used in this study are available from Muilwijk and Polyakov (2022) at the Arctic Data Center: https://doi.org/10.18739/A20P0WS23.

REFERENCES

Aagaard, K., L. K. Coachman, and E. Carmack, 1981: On the halocline of the Arctic Ocean. *Deep-Sea Res.*, **28A**, 529–545, https://doi.org/10.1016/0198-0149(81)90115-1.

Adcroft, A., and Coauthors, 2019: The GFDL global ocean and sea ice model OM4.0: Model description and simulation features. *J. Adv. Model. Earth Syst.*, **11**, 3167–3211, https://doi.org/10.1029/2019MS001726.

Amante, C., and B. W. Eakins, 2009: ETOPO1 global relief model converted to PanMap layer format. NOAA-National Geophysical Data Center, PANGAEA, accessed 1 February 2021, https://doi.org/10.1594/PANGAEA.769615.

Årthun, M., and T. Eldevik, 2016: On anomalous ocean heat transport toward the Arctic and associated climate predictability. *J. Climate*, **29**, 689–704, https://doi.org/10.1175/JCLI-D-15-0448.1.

——, ——, L. H. Smedsrud, Ø. Skagseth, and R. B. Ingvaldsen, 2012: Quantifying the influence of Atlantic heat on Barents Sea ice variability and retreat. *J. Climate*, **25**, 4736–4743, https://doi.org/10.1175/JCLI-D-11-00466.1.

Bluhm, B. A., K. N. Kosobokova, and E. C. Carmack, 2015: A tale of two basins: An integrated physical and biological perspective of the deep Arctic Ocean. *Prog. Oceanogr.*, **139**, 89–121, https://doi.org/10.1016/j.pocean.2015.07.011

——, and Coauthors, 2020: The Pan-Arctic continental slope: Sharp gradients of physical processes affect pelagic and benthic ecosystems. *Front. Mar. Sci.*, **7**, 544386, https://doi.org/10.3389/fmars.2020.544386.

Bourgain, P., and J. C. Gascard, 2011: The Arctic Ocean halocline and its interannual variability from 1997 to 2008. *Deep-Sea Res. I*, **58**, 745–756, https://doi.org/10.1016/j.dsr.2011.05.001.

Carmack, E. C., 2007: The alpha/beta ocean distinction: A perspective on freshwater fluxes, convection, nutrients, and productivity in high-latitude seas. *Deep-Sea Res. II*, **54**, 2578–2598, https://doi.org/10.1016/j.dsr2.2007.08.018.

——, and Coauthors, 2015: Towards quantifying the increasing role of oceanic heat in sea ice loss in the new Arctic. *Bull. Amer. Meteor. Soc.*, **96**, 2079–2105, https://doi.org/10.1175/BAMS-D-13-00177.1.

——, and Coauthors, 2016: Freshwater and its role in the Arctic marine system: Sources, disposition, storage, export, and physical and biogeochemical consequences in the Arctic and global oceans. *J. Geophys. Res. Biogeosci.*, **121**, 675–717, https://doi.org/10.1002/2015JG003140.

Cohen, J., and Coauthors, 2020: Divergent consensuses on Arctic amplification influence on midlatitude severe winter weather. *Nat. Climate Change*, **10**, 20–29, https://doi.org/10.1038/s41558-019-0662-y.

Cornish, S. B., Y. Kostov, H. L. Johnson, and C. Lique, 2020: Response of Arctic freshwater to the Arctic oscillation in coupled climate models. *J. Climate*, **33**, 2533–2555, https://doi.org/10.1175/JCLI-D-19-0685.1.

Danabasoglu, G., and Coauthors, 2020: The Community Earth System Model version 2 (CESM2). *J. Adv. Model. Earth Syst.*, **12**, e2019MS001916, https://doi.org/10.1029/2019MS001916.

Davis, P. E. D., C. Lique, H. L. Johnson, and J. D. Guthrie, 2016: Competing effects of elevated vertical mixing and increased freshwater input on the stratification and sea ice cover in a changing Arctic Ocean. *J. Phys. Oceanogr.*, **46**, 1531–1553, https://doi.org/10.1175/JPO-D-15-0174.1.

Davy, R., and S. Outten, 2020: The Arctic surface climate in CMIP6: Status and developments since CMIP5. *J. Climate*, **33**, 8047–8068, https://doi.org/10.1175/JCLI-D-19-0990.1.

Döscher, R., and Coauthors, 2021: The EC-Earth3 Earth system model for the Climate Model Intercomparison Project 6. *Geosci. Model Dev.*, **15**, 2973–3020, https://doi.org/10.5194/gmd-15-2973-2022.

Dunne, J. P., and Coauthors, 2020: The GFDL Earth System Model version 4.1 (GFDL-ESM 4.1): Overall coupled model description and simulation characteristics. *J. Adv. Model. Earth Syst.*, **12**, e2019MS002015, https://doi.org/10.1029/2019MS002015.

Eyring, V., S. Bony, G. A. Meehl, C. A. Senior, B. Stevens, R. J. Stouffer, and K. E. Taylor, 2016: Overview of the Coupled Model Intercomparison Project phase 6 (CMIP6) experimental design and organization. *Geosci. Model Dev.*, **9**, 1937–1958, https://doi.org/10.5194/gmd-9-1937-2016.

Giles, K. A., S. W. Laxon, A. L. Ridout, D. J. Wingham, and S. Bacon, 2012: Western Arctic Ocean freshwater storage

increased by wind-driven spin-up of the Beaufort Gyre. *Nat. Geosci.*, **5**, 194–197, https://doi.org/10.1038/ngeo1379.

Gorshkov, S. G., 1980: *Arctic Ocean*. Vol 3, *World Ocean Atlas 1980*, Ministry of Defence of the USSR, 184 pp.

Haine, T. W. N., 2020: Arctic Ocean freshening linked to anthropogenic climate change: All hands on deck. *Geophys. Res. Lett.*, **47**, e2020GL090678, https://doi.org/10.1029/2020GL090678.

——, and Coauthors, 2015: Arctic freshwater export: Status, mechanisms, and prospects. *Global Planet. Change*, **125**, 13–35, https://doi.org/10.1016/j.gloplacha.2014.11.013.

Held, I. M., and B. J. Soden, 2006: Robust responses of the hydrological cycle to global warming. *J. Climate*, **19**, 5686–5699, https://doi.org/10.1175/JCLI3990.1.

Heuzé, C., 2021: Antarctic Bottom Water and North Atlantic Deep Water in CMIP6 models. *Ocean Sci.*, **17**, 59–90, https://doi.org/10.5194/os-17-59-2021.

——, H. Zanowski, S. Karam, and M. Muilwijk, 2023: The deep Arctic Ocean and Fram Strait in CMIP6 models. *J. Climate*, https://doi.org/10.1175/JCLI-D-22-0194.1, in press.

Holland, M. M., J. Finnis, A. P. Barrett, and M. C. Serreze, 2007: Projected changes in Arctic Ocean freshwater budgets. *J. Geophys. Res.*, **112**, G04S55, https://doi.org/10.1029/2006JG000354.

Holmes, R. M., and Coauthors, 2012: Seasonal and annual fluxes of nutrients and organic matter from large rivers to the Arctic Ocean and surrounding seas. *Estuaries Coasts*, **35**, 369–382, https://doi.org/10.1007/s12237-011-9386-6.

Ilicak, M., and Coauthors, 2016: An assessment of the Arctic Ocean in a suite of interannual CORE-II simulations. Part III: Hydrography and fluxes. *Ocean Modell.*, **100**, 141–161, https://doi.org/10.1016/j.ocemod.2016.02.004.

IPCC, 2021: *Climate Change 2021: The Physical Science Basis*. Cambridge University Press, 2391 pp.

Jahn, A., and R. Laiho, 2020: Forced changes in the Arctic freshwater budget emerge in the early 21st century. *Geophys. Res. Lett.*, **47**, e2020GL088854, https://doi.org/10.1029/2020GL088854.

Kattsov, V. M., J. E. Walsh, W. L. Chapman, V. A. Govorkova, T. V. Pavlova, and X. Zhang, 2007: Simulation and projection of Arctic freshwater budget components by the IPCC AR4 global climate models. *J. Hydrometeor.*, **8**, 571–589, https://doi.org/10.1175/JHM575.1.

Kelley, M., and Coauthors, 2020: GISS-E2.1: Configurations and climatology. *J. Adv. Model. Earth Syst.*, **12**, e2019MS002025, https://doi.org/10.1029/2019MS002025.

Khosravi, N., Q. Wang, N. Koldunov, C. Hinrichs, T. Semmler, S. Danilov, and T. Jung, 2022: The Arctic Ocean in CMIP6 models: Biases and projected changes in temperature and salinity. *Earth's Future*, **10**, e2021EF002282, https://doi.org/10.1029/2021EF002282.

Li, G., L. Cheng, J. Zhu, K. E. Trenberth, M. E. Mann, and J. P. Abraham, 2020: Increasing ocean stratification over the past half-century. *Nat. Climate Change*, **10**, 1116–1123, https://doi.org/10.1038/s41558-020-00918-2.

Lique, C., H. L. Johnson, and Y. Plancherel, 2018: Emergence of deep convection in the Arctic Ocean under a warming climate. *Climate Dyn.*, **50**, 3833–3847, https://doi.org/10.1007/s00382-017-3849-9.

Lurton, T., and Coauthors, 2020: Implementation of the CMIP6 forcing data in the IPSL-CM6A-LR model. *J. Adv. Model. Earth Syst.*, **12**, e2019MS001940, https://doi.org/10.1029/2019MS001940.

McDougall, T. J., and P. M. Barker, 2011: Getting started with TEOS-10 and the Gibbs Seawater (GSW) Oceanographic Toolbox. SCOR/IAPSO, 28 pp., http://www.teos-10.org/pubs/gsw/v3_04/pdf/Getting_Started.pdf.

Metzner, E. P., M. Salzmann, and R. Gerdes, 2020: Arctic Ocean surface energy flux and the cold halocline in future climate projections. *J. Geophys. Res. Oceans*, **125**, e2019JC015554, https://doi.org/10.1029/2019JC015554.

Muilwijk, M., and I. V. Polyakov, 2022: Vertical profiles of temperature and salinity in the central Arctic Ocean from observations and 13 CMIP6 models—1970–2017. Arctic Data Center, accessed 3 November 2022, https://doi.org/10.18739/A20P0WS23.

——, and Coauthors, 2019: Arctic Ocean response to Greenland Sea wind anomalies in a suite of model simulations. *J. Geophys. Res. Oceans*, **124**, 6286–6322, https://doi.org/10.1029/2019JC015101.

Müller, W. A., and Coauthors, 2018: A higher-resolution version of the Max Planck Institute Earth system model (MPI-ESM1.2-HR). *J. Adv. Model. Earth Syst.*, **10**, 1383–1413, https://doi.org/10.1029/2017MS001217.

Nansen, F., 1902: *The Oceanography of the North Polar Basin*. Vol. 3. Longmans, Green, and Company, 427 pp.

Nguyen, A. T., D. Menemenlis, and R. Kwok, 2009: Improved modeling of the Arctic halocline with a subgrid-scale brine rejection parameterization. *J. Geophys. Res.*, **114**, C11014, https://doi.org/10.1029/2008JC005121.

Notz, D., and SIMIP Community, 2020: Arctic sea ice in CMIP6. *Geophys. Res. Lett.*, **47**, e2019GL086749, https://doi.org/10.1029/2019GL086749.

Nummelin, A., C. Li, and L. H. Smedsrud, 2015: Response of Arctic Ocean stratification to changing river runoff in a column model. *J. Geophys. Res. Oceans*, **120**, 2655–2675, https://doi.org/10.1002/2014JC010571.

——, M. Ilicak, C. Li, and L. H. Smedsrud, 2016: Consequences of future increased Arctic runoff on Arctic Ocean stratification, circulation, and sea ice cover. *J. Geophys. Res. Oceans*, **121**, 617–637, https://doi.org/10.1002/2015JC011156.

O'Neill, B. C., and Coauthors, 2016: The Scenario Model Intercomparison Project (ScenarioMIP) for CMIP6. *Geosci. Model Dev.*, **9**, 3461–3482, https://doi.org/10.5194/gmd-9-3461-2016.

Onarheim, I. H., T. Eldevik, M. Årthun, R. B. Ingvaldsen, and L. H. Smedsrud, 2015: Skillful prediction of Barents Sea ice cover. *Geophys. Res. Lett.*, **42**, 5364–5371, https://doi.org/10.1002/2015GL064359.

Peralta-Ferriz, C., and R. A. Woodgate, 2015: Seasonal and interannual variability of pan-Arctic surface mixed layer properties from 1979 to 2012 from hydrographic data, and the dominance of stratification for multiyear mixed layer depth shoaling. *Prog. Oceanogr.*, **134**, 19–53, https://doi.org/10.1016/j.pocean.2014.12.005.

Peterson, B. J., R. M. Holmes, J. W. McClelland, C. J. Vörösmarty, R. B. Lammers, A. I. Shiklomanov, I. A. Shiklomanov, and S. Rahmstorf, 2002: Increasing river discharge to the Arctic Ocean. *Science*, **298**, 2171–2173, https://doi.org/10.1126/science.1077445.

Polyakov, I. V., and Coauthors, 2017: Greater role for Atlantic inflows on sea-ice loss in the Eurasian Basin of the Arctic Ocean. *Science*, **356**, 285–291, https://doi.org/10.1126/science.aai8204.

——, A. V. Pnyushkov, and E. C. Carmack, 2018: Stability of the Arctic halocline: A new indicator of Arctic climate change. *Environ. Res. Lett.*, **13**, 125008, https://doi.org/10.1088/1748-9326/aaec1e.

——, and Coauthors, 2020a: Borealization of the Arctic Ocean in response to anomalous advection from sub-Arctic seas. *Front. Mar. Sci.*, **7**, 491, https://doi.org/10.3389/fmars.2020.00491.

——, and Coauthors, 2020b: Weakening of cold halocline layer exposes sea ice to oceanic heat in the eastern Arctic Ocean. *J. Climate*, **33**, 8107–8123, https://doi.org/10.1175/JCLI-D-19-0976.1.

Proshutinsky, A., R. H. Bourke, and F. A. McLaughlin, 2002: The role of the Beaufort Gyre in Arctic climate variability: Seasonal to decadal climate scales. *Geophys. Res. Lett.*, **29**, 2100, https://doi.org/10.1029/2002GL015847.

——, and Coauthors, 2009: Beaufort Gyre freshwater reservoir: State and variability from observations. *J. Geophys. Res.*, **114**, C00A10, https://doi.org/10.1029/2008JC005104.

——, and Coauthors, 2019: Analysis of the Beaufort Gyre freshwater content in 2003–2018. *J. Geophys. Res. Oceans*, **124**, 9658–9689, https://doi.org/10.1029/2019JC015281.

Rabe, B., and Coauthors, 2011: An assessment of Arctic Ocean freshwater content changes from the 1990s to the 2006–2008 period. *Deep-Sea Res. I*, **58**, 173–185, https://doi.org/10.1016/j.dsr.2010.12.002.

——, and Coauthors, 2014: Arctic Ocean basin liquid freshwater storage trend 1992–2012. *Geophys. Res. Lett.*, **41**, 961–968, https://doi.org/10.1002/2013GL058121.

——, and Coauthors, 2022: Overview of the MOSAiC expedition: Physical oceanography. *Elementa*, **10**, 00062, https://doi.org/10.1525/elementa.2021.00062.

Randelhoff, A., J. Holding, M. Janout, M. K. Sejr, M. Babin, J.-E. Tremblay, and M. B. Alkire, 2020: Pan-Arctic Ocean primary production constrained by turbulent nitrate fluxes. *Front. Mar. Sci.*, **7**, 150, https://doi.org/10.3389/fmars.2020.00150.

Rosenblum, E., R. Fajber, J. C. Stroeve, S. T. Gille, L. B. Tremblay, and E. C. Carmack, 2021: Surface salinity under transitioning ice cover in the Canada Basin: Climate model biases linked to vertical distribution of fresh water. *Geophys. Res. Lett.*, **48**, e2021GL094739, https://doi.org/10.1029/2021GL094739.

Rudels, B., 2015: Arctic Ocean circulation, processes and water masses: A description of observations and ideas with focus on the period prior to the International Polar Year 2007–2009. *Prog. Oceanogr.*, **132**, 22–67, https://doi.org/10.1016/j.pocean.2013.11.006.

——, E. P. Jones, U. Schauer, and P. Eriksson, 2004: Atlantic sources of the Arctic Ocean surface and halocline waters. *Polar Res.*, **23**, 181–208, https://doi.org/10.3402/polar.v23i2.6278.

Seland, Ø., and Coauthors, 2020: The Norwegian Earth system model, NorESM2—Evaluation of the CMIP6 DECK and historical simulations. *Geosci. Model Dev. Discuss.*, https://doi.org/10.5194/gmd-2019-378.

Sellar, A. A., and Coauthors, 2020: Implementation of U.K. Earth system models for CMIP6. *J. Adv. Model. Earth Syst.*, **12**, e2019MS001946, https://doi.org/10.1029/2019MS001946.

Serreze, M. C., and Coauthors, 2006: The large-scale freshwater cycle of the Arctic. *J. Geophys. Res.*, **111**, C11010, https://doi.org/10.1029/2005JC003424.

Shen, Z., A. Duan, D. Li, and J. Li, 2021: Assessment and ranking of climate models in Arctic sea ice cover simulation: From CMIP5 to CMIP6. *J. Climate*, **34**, 3609–3627, https://doi.org/10.1175/JCLI-D-20-0294.1.

Shepherd, A., and Coauthors, 2020: Mass balance of the Greenland Ice Sheet from 1992 to 2018. *Nature*, **579**, 233–239,https://doi.org/10.1038/s41586-019-1855-2.

Shu, Q., F. Qiao, Z. Song, J. Zhao, and X. Li, 2018: Projected freshening of the Arctic Ocean in the 21st century. *J. Geophys. Res. Oceans*, **123**, 9232–9244, https://doi.org/10.1029/2018JC014036.

——, Q. Wang, J. Su, X. Li, and F. Qiao, 2019: Assessment of the Atlantic water layer in the Arctic Ocean in CMIP5 climate models. *Climate Dyn.*, **53**, 5279–5291, https://doi.org/10.1007/s00382-019-04870-6.

——, ——, Z. Song, F. Qiao, J. Zhao, M. Chu, and X. Li, 2020: Assessment of sea ice extent in CMIP6 with comparison to observations and CMIP5. *Geophys. Res. Lett.*, **47**, e2020GL087965, https://doi.org/10.1029/2020GL087965.

Smedsrud, L. H., and Coauthors, 2022: Nordic seas heat loss, Atlantic inflow, and Arctic Sea ice cover over the last century. *Rev. Geophys.*, **60**, e2020RG000725, https://doi.org/10.1029/2020RG000725.

Solomon, A., and Coauthors, 2021: Freshwater in the Arctic Ocean 2010–2019. *Ocean Sci.*, **17**, 1081–1102, https://doi.org/10.5194/os-17-1081-2021.

Steele, M., G. L. Mellor, and M. G. McPhee, 1989: Role of the molecular sublayer in the melting or freezing of sea ice. *J. Phys. Oceanogr.*, **19**, 139–147, https://doi.org/10.1175/1520-0485(1989)019<0139:ROTMSI>2.0.CO;2.

——, J. Morison, W. Ermold, I. Rigor, M. Ortmeyer, and K. Shimada, 2004: Circulation of summer Pacific halocline water in the Arctic Ocean. *J. Geophys. Res.*, **109**, C02027, https://doi.org/10.1029/2003JC002009.

Stroeve, J., and D. Notz, 2018: Changing state of Arctic sea ice across all seasons. *Environ. Res. Lett.*, **13**, 103001, https://doi.org/10.1088/1748-9326/aade56.

Swart, N. C., and Coauthors, 2019: The Canadian Earth System Model version 5 (CanESM5.0.3). *Geosci. Model Dev.*, **12**, 4823–4873, https://doi.org/10.5194/gmd-12-4823-2019.

Tailleux, R., 2009: Understanding mixing efficiency in the oceans: Do the nonlinearities of the equation of state for seawater matter? *Ocean Sci.*, **5**, 271–283, https://doi.org/10.5194/os-5-271-2009.

Tatebe, H., and Coauthors, 2019: Description and basic evaluation of simulated mean state, internal variability, and climate sensitivity in MIROC6. *Geosci. Model Dev.*, **12**, 2727–2765, https://doi.org/10.5194/gmd-12-2727-2019.

Timmermans, M.-L., and J. Marshall, 2020: Understanding Arctic Ocean circulation: A review of ocean dynamics in a changing climate. *J. Geophys. Res. Oceans*, **125**, e2018JC014378, https://doi.org/10.1029/2018JC014378.

Timokhov, L., and F. Tanis, Eds., 1997: Environmental Working Group Joint U.S.–Russian Atlas of the Arctic Ocean, version 1, Distributed by National Snow and Ice Data Center, accessed 1 February 2021, https://nsidc.org/data/g01961/versions/1.

Treshnikov, A. F., 1985: *Arctic Atlas*. Head Administration of Geodesy and Cartography of the Soviet Ministry, 204 pp.

Tsubouchi, T., K. Våge, B. Hansen, K. M. H. Larsen, S. Østerhus, C. Johnson, S. Jónsson, and H. Valdimarsson, 2021: Increased ocean heat transport into the Nordic seas and Arctic Ocean over the period 1993–2016. *Nat. Climate Change*, **11**, 21–26, https://doi.org/10.1038/s41558-020-00941-3.

Tsujino, H., and Coauthors, 2020: Evaluation of global ocean–sea-ice model simulations based on the experimental protocols of the Ocean Model Intercomparison Project phase 2 (OMIP-2). *Geosci. Model Dev.*, **13**, 3643–3708, https://doi.org/10.5194/gmd-13-3643-2020.

Wang, S., Q. Wang, M. Wang, G. Lohmann, and F. Qiao, 2022: Arctic Ocean freshwater in CMIP6 coupled models. *Earth's Future*, **10**, e2022EF002878, https://doi.org/10.1029/2022EF002878.

Wang, Q., and Coauthors, 2016: An assessment of the Arctic Ocean in a suite of interannual CORE-II simulations. Part II: Liquid freshwater. *Ocean Modell.*, **99**, 86–109, https://doi.org/10.1016/j.ocemod.2015.12.009.

——, J. Marshall, J. Scott, G. Meneghello, S. Danilov, and T. Jung, 2019: On the feedback of ice–ocean stress coupling from geostrophic currents in an anticyclonic wind regime over the Beaufort Gyre. *J. Phys. Oceanogr.*, **49**, 369–383, https://doi.org/10.1175/JPO-D-18-0185.1.

Woodgate, R. A., K. Aagaard, J. H. Swift, K. K. Falkner, and W. M. Smethie Jr., 2005: Pacific ventilation of the Arctic Ocean's lower halocline by upwelling and diapycnal mixing over the continental margin. *Geophys. Res. Lett.*, **32**, L18609, https://doi.org/10.1029/2005GL023999.

——, T. J. Weingartner, and R. Lindsay, 2012: Observed increases in Bering Strait oceanic fluxes from the Pacific to the Arctic from 2001 to 2011 and their impacts on the Arctic Ocean water column. *Geophys. Res. Lett.*, **39**, L24603, https://doi.org/10.1029/2012GL054092.

Wu, T., and Coauthors, 2019: The Beijing Climate Center Climate System Model (BCC-CSM): The main progress from CMIP5 to CMIP6. *Geosci. Model Dev.*, **12**, 1573–1600, https://doi.org/10.5194/gmd-12-1573-2019.

Xin-Yao, R., L. I. Jian, C. Hao-Ming, X. I. N. Yu-Fei, S. U. Jing-Zhi, and H. U. A. Li-Juan, 2019: Introduction of CAMS-CSM model and its participation in CMIP6. *Climate Change Res.*, **15**, 540–544, https://doi.org/10.12006/j.issn.1673-1719.2019.186.

Yasunaka, S., and Coauthors, 2018: Arctic ocean CO_2 uptake: An improved multiyear estimate of the air–sea CO_2 flux incorporating chlorophyll a concentrations. *Biogeosciences*, **15**, 1643–1661, https://doi.org/10.5194/bg-15-1643-2018.

Yukimoto, S., and Coauthors, 2019: The Meteorological Research Institute Earth System Model version 2.0, MRI-ESM2.0: Description and basic evaluation of the physical component. *J. Meteor. Soc. Japan*, **97**, 931–965, https://doi.org/10.2151/jmsj.2019-051.

Zanowski, H., A. Jahn, and M. M. Holland, 2021: Arctic Ocean freshwater in CMIP6 ensembles: Declining sea ice, increasing ocean storage and export. *J. Geophys. Res. Oceans*, **126**, e2020JC016930, https://doi.org/10.1029/2020JC016930.